

UNCLASSIFIED

AD NUMBER

**AD489981**

NEW LIMITATION CHANGE

TO

**Approved for public release, distribution  
unlimited**

FROM

**Distribution authorized to U.S. Gov't.  
agencies and their contractors; Critical  
Technology; SEP 1966. Other requests shall  
be referred to Ballistic Systems and Space  
Systems Division, Los Angeles, CA.**

AUTHORITY

**SAMSO ltr, 19 Jan 1972**

THIS PAGE IS UNCLASSIFIED

100  
100  
100  
100  
100  
100

# Lifting Reentry Communications

## Volume II: Systems Calculations

---

**SEPTEMBER 1966**

---

Prepared by  
REENTRY AND PLASMA-ELECTROMAGNETICS DEPARTMENT  
Plasma Research Laboratory  
Labs Division  
Laboratory Operations  
AEROSPACE CORPORATION

Prepared for BALLISTIC SYSTEMS AND SPACE SYSTEMS DIVISIONS  
AIR FORCE SYSTEMS COMMAND  
LOS ANGELES AIR FORCE STATION  
Los Angeles, California

Best Available Copy

NOTICE

This document is subject to special export controls and each transmittal to foreign governments or foreign nationals may be made only with prior approval of SSD(SSTRT).

Air Force Report No.  
SSD-TR-66-73, Vol II

Aerospace Report No.  
TR-669(6220-10)-3, Vol II

LIFTING REENTRY COMMUNICATIONS  
VOLUME II: SYSTEMS CALCULATIONS

Prepared by  
REENTRY AND PLASMA-ELECTROMAGNETICS DEPARTMENT  
Plasma Research Laboratory

Laboratories Division  
Laboratory Operations  
AEROSPACE CORPORATION

September 1966

Prepared for  
BALLISTIC SYSTEMS AND SPACE SYSTEMS DIVISIONS  
AIR FORCE SYSTEMS COMMAND  
LOS ANGELES AIR FORCE STATION  
Los Angeles, California

## FOREWORD

This report is published by the Aerospace Corporation, El Segundo, California, under Air Force Contract No. AF 04(695)-669. The report was authored by the following members of the ad hoc Working Group on Reentry Communications:

Donald M. Dix  
Kurt E. Golden  
Edward C. Taylor  
Marc A. Kolpin  
Paul R. Caron

This working group was organized by Richard H. Huddlestone, Head, Reentry and Plasma-Electromagnetics Department, Plasma Research Laboratory in anticipation of the requirements of the Space Systems Division. The authors gratefully acknowledge Dr. Huddlestone's many suggestions and his constructive criticism.

The following figures have been adapted as indicated: Fig. B-5, from Ref. B-4; Fig. B-6, from Ref. B-5; Fig. B-7, from Ref. B-6; Fig. B-8, from Refs. B-7 and B-8; and Fig. H-1, from Ref. H-1.

This report, which documents research carried out from 1 July 1965 through 1 February 1966, was submitted on 20 September 1966 to Capt. R. F. Jones, SSTRT, for review and approval.

Information in this report is embargoed under the U. S. Export Control Act of 1949, administered by the Department of Commerce. This report may be released by departments or agencies of the U. S. Government to departments or agencies of foreign governments with which the United States has defense treaty commitments. Private individuals or firms must comply with Department of Commerce export control regulations.

Approved

*R. X. Meyer*  
R. X. Meyer, Director  
Plasma Research Laboratory  
Laboratories Division  
Laboratory Operations

Publication of this report does not constitute Air Force approval of the report's findings or conclusions. It is published only for the exchange and stimulation of ideas.

*Robert F. Jones*  
Robert F. Jones, Captain  
Space Systems Division  
Air Force Systems Command

## ABSTRACT

Calculations supporting the lifting reentry communications systems study are described in this volume. The application and interpretation of these calculations is presented in Volume I of this report. These calculations include the study of lifting reentry trajectories, aerodynamic calculations, signal attenuation, system margins, system modifications, communications fin heat transfer, magnetic window, coolant injection, electrophilic seeding, and quasi-optical and optical systems.

## CONTENTS

<b>FOREWORD</b> .....	ii
<b>ABSTRACT</b> .....	iii
<b>INTRODUCTION</b> .....	1-1
<b>APPENDICES:</b>	
A. LIFTING REENTRY TRAJECTORIES .....	A-1
B. AERODYNAMIC CALCULATIONS .....	B-1
C. SIGNAL ATTENUATION .....	C-1
D. SYSTEM MARGINS .....	D-1
E. SYSTEM MODIFICATIONS .....	E-1
F. COMMUNICATIONS FIN HEAT TRANSFER .....	F-1
G. MAGNETIC WINDOW .....	G-1
H. COOLANT INJECTION .....	H-1
I. ELECTROPHILIC SEEDING .....	I-1
J. QUASI-OPTICAL AND OPTICAL SYSTEMS .....	J-1

## FIGURES

A-1.	Flight Geometry. . . . .	A-2
B-1.	Plasma Frequency in Air, Density . . . . .	B-2
B-2.	Plasma Frequency in Air, Temperature. . . . .	B-2
B-3.	Degree of Ionization in Air. . . . .	B-3
B-4.	Collision Frequency in Air. . . . .	B-3
B-5.	Plasma Frequency and Electron Collision Frequency in Equilibrium Air Behind Normal Shocks . . . . .	B-4
B-6.	Temperature and Density Behind Normal and Oblique Shocks . . . . .	B-5
B-7.	Normalized Blunt Body Shock Detachment $\Delta R = 2/\{3[\rho_2/(\rho_1 - 1)]\}$ . . . . .	B-5
B-8.	Shock Angle vs Body Angle for Wedges and Cones . . . . .	B-5
B-9.	Maximum Plasma Frequency in Boundary Layer: Shock Angle = 50 deg. . . . .	B-6
B-10.	Maximum Plasma Frequency in Boundary Layer: Shock Angle = 40 deg. . . . .	B-6
B-11.	Maximum Plasma Frequency in Boundary Layer: Shock Angle = 30 deg. . . . .	B-7
B-12.	Maximum Plasma Frequency in Boundary Layer: Shock Angle = 20 deg. . . . .	B-7
B-13.	Collision Frequency at Peak Boundary Layer Condition: Shock Angle = 50 deg. . . . .	B-8
B-14.	Collision Frequency at Peak Boundary Layer Condition: Shock Angle = 40 deg. . . . .	B-8
B-15.	Collision Frequency at Peak Boundary Layer Condition: Shock Angle = 30 deg. . . . .	B-9
B-16.	Collision Frequency at Peak Boundary Layer Condition: Shock Angle = 20 deg. . . . .	B-9
B-17.	Wedge Boundary Layer Thickness (Laminar): Shock Angle = 50 deg. . . . .	B-10
B-18.	Wedge Boundary Layer Thickness (Laminar): Shock Angle = 40 deg. . . . .	B-10
B-19.	Wedge Boundary Layer Thickness (Laminar): Shock Angle = 30 deg. . . . .	B-11

FIGURES (Continued)

B-20.	Wedge Boundary Layer Thickness (Laminar): Shock Angle = 20 deg. . . . .	B-11
B-21.	Boundary Layer Edge Reynolds Number (per foot) for Wedge . . . . .	B-12
D-1.	Antenna Gain vs Frequency . . . . .	D-3
D-2.	Effective Antenna Temperature . . . . .	D-3
D-3.	Typical Free Space System Margin . . . . .	D-3
G-1.	Coil Geometry . . . . .	G-1
H-1.	Cooling Effectiveness as a Function of Temperature for Various Coolants . . . . .	H-1
H-2.	Quasi One-Dimensional Mixing Process . . . . .	H-2
I-1.	Reduction of Equilibrium Electron Concentrations in Seeded Air . . . . .	I-4
I-2.	Reduction of Nonequilibrium Electron Concentrations in Seeded Ionized Gases . . . . .	I-4

TABLES

C-I.	Stagnation Point Attenuation . . . . .	C-2
C-II.	Shock Layer Attenuation, 50-deg Wedge . . . . .	C-3
C-III.	Shock Layer Attenuation, 40-deg Wedge . . . . .	C-4
C-IV.	Boundary Layer Attenuation, 40-deg Wedge . . . . .	C-5
C-V.	Shock Layer Attenuation, 30-deg Wedge . . . . .	C-6
C-VI.	Boundary Layer Attenuation, 30-deg Wedge . . . . .	C-7
C-VII.	Boundary Layer Attenuation, 20-deg Wedge . . . . .	C-8
C-VIII.	Shock Layer Attenuation, 50-deg Cone . . . . .	C-9
C-IX.	Shock Layer Attenuation, 40-deg Cone . . . . .	C-10
C-X.	Boundary Layer Attenuation, 40-deg Cone . . . . .	C-11
C-XI.	Shock Layer Attenuation, 30-deg Cone . . . . .	C-12
C-XII.	Boundary Layer Attenuation, 30-deg Cone . . . . .	C-13
C-XIII.	Boundary Layer Attenuation, 20-deg Cone . . . . .	C-14
C-XIV.	Shock Layer Thickness vs Ionization Distance for Cones and Wedges . . . . .	C-15
E-I.	Behavior of Breakdown Parameter R . . . . .	E-2
H-I.	Species Concentration in Air . . . . .	H-6
H-II.	Evaporation Times, Free Molecular Flow . . . . .	H-6

## 1. INTRODUCTION

This report is the second of three volumes describing the analysis of lifting reentry communications systems. This volume contains the details of investigations that form the basis of the argument in Volume I; Volume III contains an extensive tabulation of transmission and reflection coefficients for a plasma slab.

Each investigation presented in this report has been specifically referred to in Volume I as an appendix, Appendices A through J. These analyses are intended to have meaning only in the context of the total argument presented in Volume I, and this relationship is emphasized in each section of this volume.

## APPENDIX A

### LIFTING REENTRY TRAJECTORIES

This appendix gives a short derivation of the equations of motion of a gliding reentry vehicle and discusses the assumptions made to obtain the trajectories shown in Figs. 1 through 3 of Volume I, Section II-A-1.

#### 1. EQUATIONS OF MOTION

The flight geometry is illustrated in Fig. A-1. The pertinent symbols are

$C_D$  = drag coefficient

$C_L$  = lift coefficient

$D$  = aerodynamic drag

$g$  = acceleration of gravity, assumed constant

$H$  = altitude above earth surface

$L$  = aerodynamic lift

$M$  = Mach number

$m$  = mass of the R/V

$\bar{R}$  = earth radius

$r$  = radial position of vehicle from center of earth

$Re$  = Reynolds number

$S$  = aerodynamic reference area

$T$  = local temperature

$U$  = magnitude of velocity vector

$U_0 = \text{orbital velocity} (r_0 g)^{1/2}$

$W$  = weight of vehicle

$\alpha$  = angle of attack of R/V

$\theta$  = path angle

$\rho$  = local density

$\rho_s$  = density at sea level

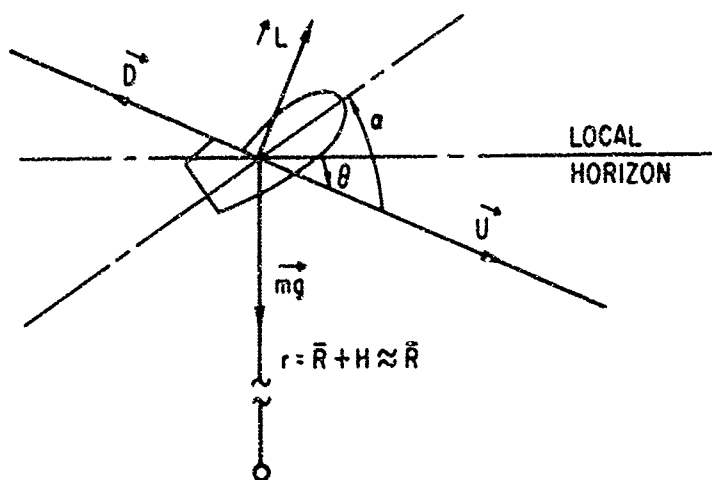


Fig. A-1. Flight Geometry

The definitions

$$L = SC_L \rho U^2 / 2 \quad (A-1)$$

and

$$D = SC_D \rho U^2 / 2 \quad (A-2)$$

lead to the equations of motion

$$- \frac{dU}{dt} = - g \sin \theta + \frac{C_D S}{m} \rho \frac{U^2}{2} \quad (A-3)$$

and

$$U \frac{d\theta}{dt} = g \cos \theta - \frac{U^2 \cos \theta}{r} - \frac{C_L S \rho U^2}{2m} \quad (A-4)$$

The initial conditions are  $t = 0$ ,  $U = U_0$ ,  $\theta = \theta_0$ , and  $H = H_0$ .

The relation  $\rho(H)$  may be taken from a standard atmosphere table or be approximated by the isothermal atmosphere

$$\frac{\rho}{\rho_s} = \exp[-(g/RT)H] \quad (A-5)$$

The dependence of  $C_D$  and  $C_L$  on  $a$ ,  $Re$ , and  $M$  must be determined for the particular geometry under consideration. The altitude of the R/V as a function of time is given by

$$H = H_0 - \int_0^t U \sin \theta \, dt \quad (A-6)$$

## 2. EQUILIBRIUM TRAJECTORY

An equilibrium lifting reentry trajectory is characterized by a small path angle and a small rate of change in the path angle. Under these circumstances, the equations of motion become

$$\frac{dU}{dt} = \frac{-C_D S}{m} \rho \frac{U^2}{2} \quad (A-7)$$

and

$$\frac{U}{U_0} = \left[ \frac{r/r_0}{i + r(C_L S/m)(\rho/2)} \right]^{1/2} \quad (A-8)$$

If we introduce  $\rho = \rho_s \exp[-(g/RT)H]$ , the velocity can be computed as a function of altitude from Eq. (A-8). Integration of Eq. (A-7) will give  $t(U)$ . For  $r = r_0 = \text{constant}$ , the integration yields

$$t - t_i = \frac{U_0}{2g} \frac{L}{D} \ln \left\{ \frac{[1 + (U_i/U_0)]}{[1 - (U_i/U_0)]} \frac{[1 - (U/U_0)]}{[1 + (U/U_0)]} \right\} \quad (\text{A-9})$$

Trajectory 1 of Fig. 2, Volume I, has been computed from Eqs. (A-8) and (A-9) using the ARDC Atmosphere Tables.<sup>1</sup> Trajectory 1 corresponds to an entry with  $U_0 = 25.6 \text{ kft/sec}$ ,  $\theta = 0$ , and a ballistic parameter  $W/C_L S$  of  $200 \text{ lb/ft}^2$ .

### 3. NONEQUILIBRIUM TRAJECTORY

As illustrated by Fig. 1, Volume I, a nonzero initial path angle leads to oscillations of the trajectory in the altitude vs velocity plane. To consider the increased depth of blackout encountered during the low-altitude high-velocity pullout, we have defined an idealized and rather extreme nonequilibrium trajectory which is the envelope of trajectories computed by numerically integrating Eqs. (A-3) and (A-4) for  $\theta_0 \neq 0$  and  $W/C_L A = 200 \text{ lb/ft}^2$ . The corresponding time scale was determined by observing that the time elapsed from the reentry point is approximately independent of altitude.

---

<sup>1</sup> The numerical integration of Eqs. (A-7) and (A-8) was originally performed by the General Dynamics Corp., Fort Worth, and the results made available to us by Mr. W. C. Melton of ESTO, Aerospace Corp.

## APPENDIX B

### AERODYNAMIC CALCULATIONS

This appendix is a compilation of results obtained by the methods described in Volume I, Section II-A-3.

#### 1. OUTER INVISCID FLOW

Figures B-1 through B-4 show the plasma frequency, degree of ionization, and collision frequency in equilibrium air. The plasma frequency and degree of ionization are taken from work by Bleviss (Ref. B-1), which was based on the results of Logan and Treanor (Ref. B-2). The collision frequency was obtained from Bachynski, et al. (Ref. B-3).

Figures B-5 through B-8 show inviscid shock layer properties for cones, wedges, and axisymmetric stagnation points. These figures were adapted as follows: Fig. B-5 from Ref. B-4; Fig. B-6 from Ref. B-5; Fig. B-7 from Ref. B-6; and Fig. B-8 from Refs. B-7 and B-8.

#### 2. VISCOUS BOUNDARY LAYER

The boundary layer properties were obtained from an existing computer program that is described in Ref. B-8. The maximum plasma frequency in the boundary layer on cones and wedges is presented in Figs. B-9 through B-12. Figures B-13 through B-16 show the collision frequency. It is to be noted that these properties differ by as much as 50%, from the best available data (see Volume I, II-A-3). The normalized boundary layer thickness  $\delta/(x)^{-1/2}$  for wedges is shown in Figs. B-17 through B-20 (The boundary layer thickness in inches is  $\delta$ , and the distance along the surface of the vehicle measured from the nose in feet is  $x$ ); the conical boundary layer thickness is less by a factor of  $(3)^{-1/2}$ . Figure B-21 presents representative values of the Reynolds number at the boundary layer edge.

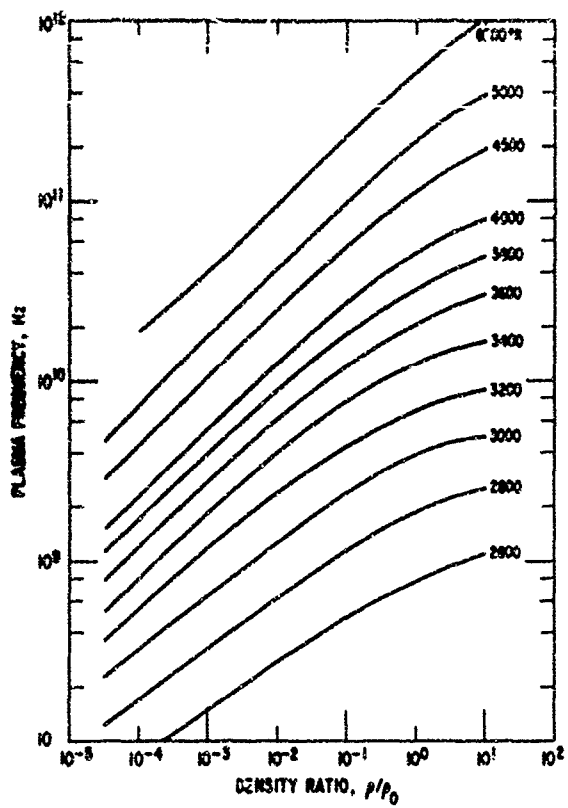


Fig. B-1. Plasma Frequency  
in Air, Density

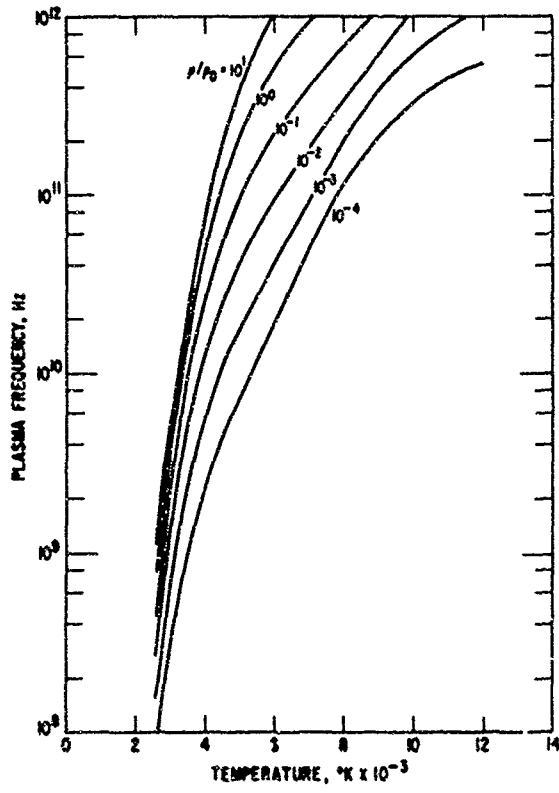


Fig. B-2. Plasma Frequency  
in Air, Temperature

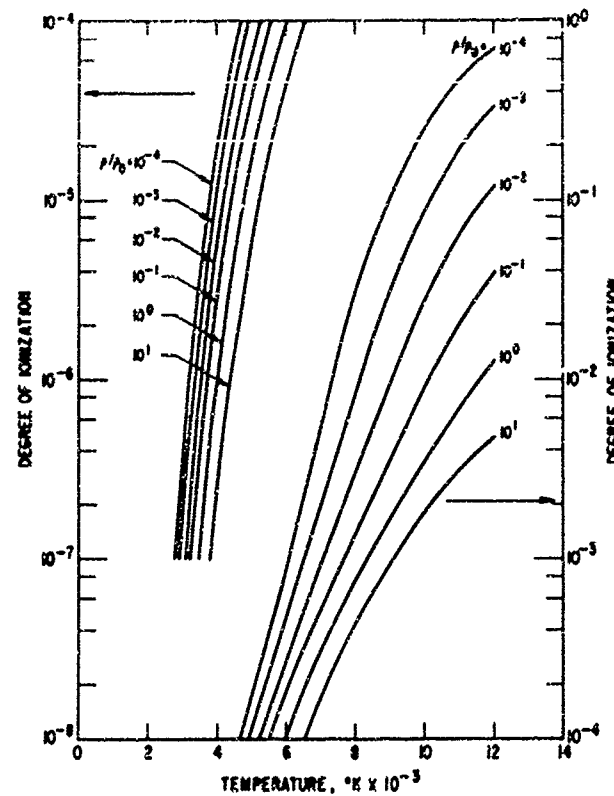


Fig. B-3. Degree of Ionization in Air

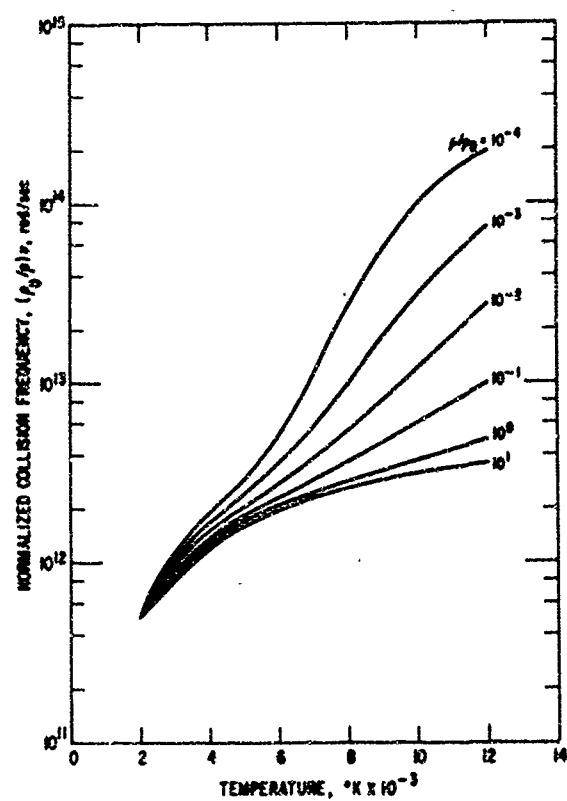


Fig. B-4. Collision Frequency in Air

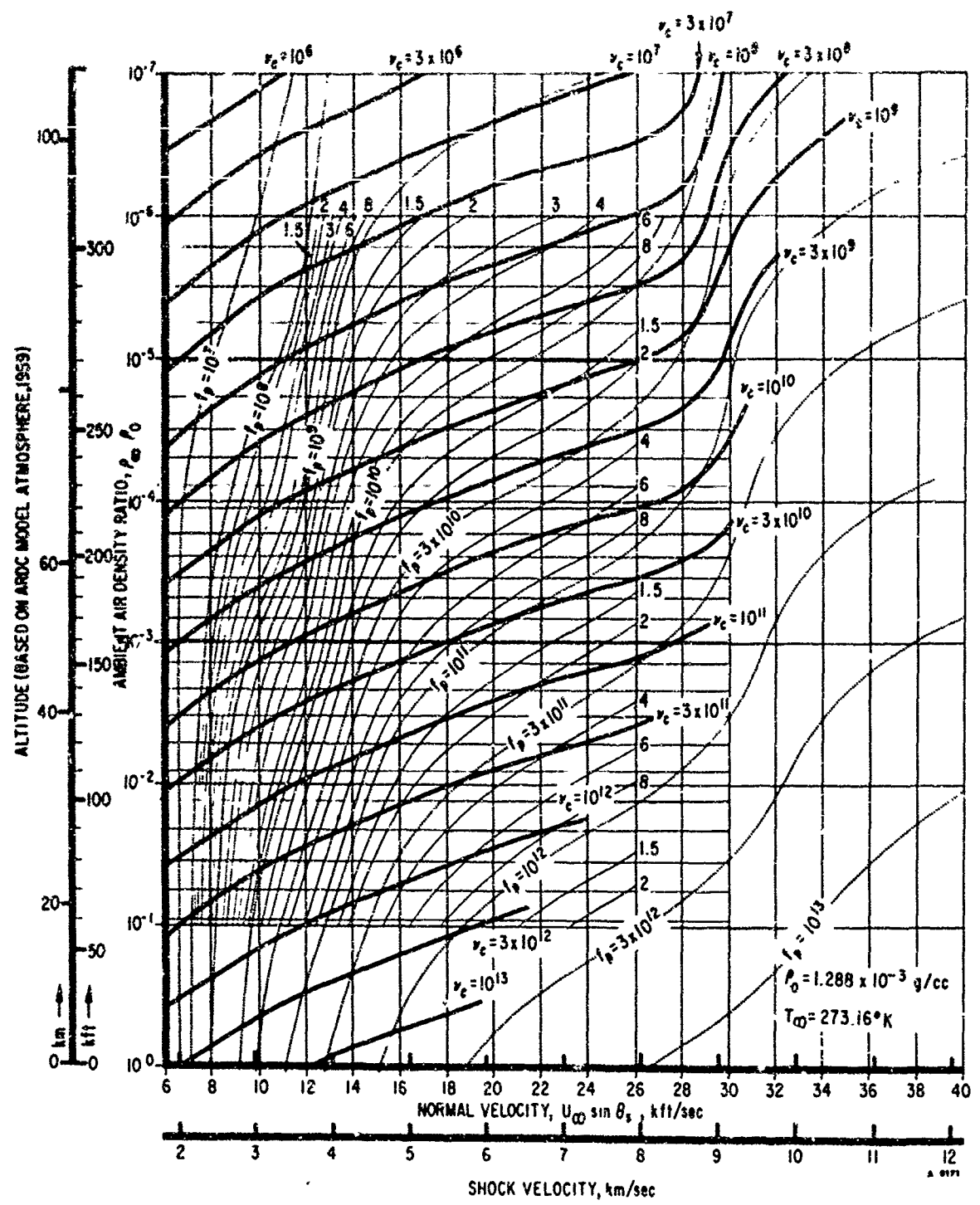


Fig. B-5: Plasma Frequency and Electron Collision Frequency in Equilibrium Air Behind Normal Shocks

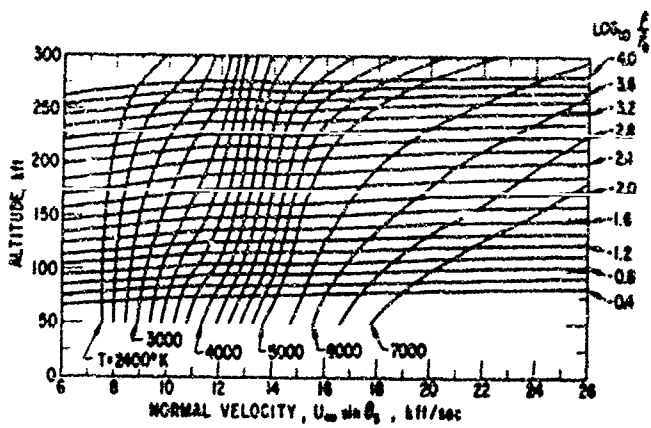


Fig. B-6. Temperature and Density Behind Normal and Oblique Shocks

Fig. B-7. Normalized Blunt Body Shock Detachment  
 $\Delta R = 2/\{3[\rho_2/(\rho_1 - 1)]\}$

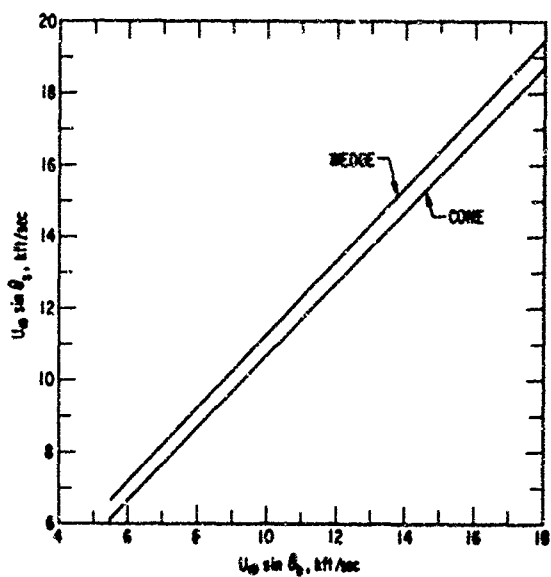
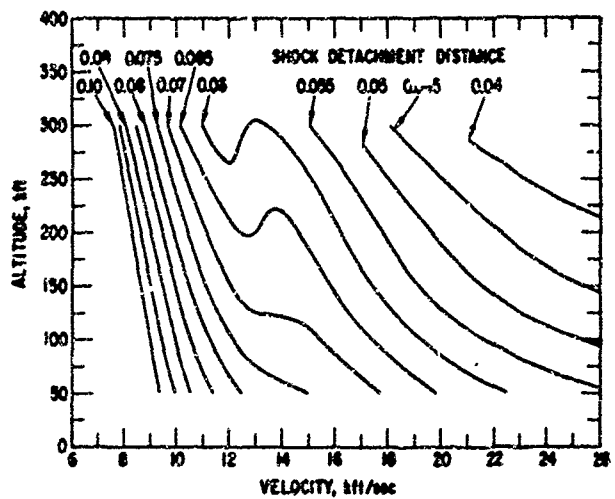


Fig. B-8. Shock Angle vs Body Angle for Wedges and Cones

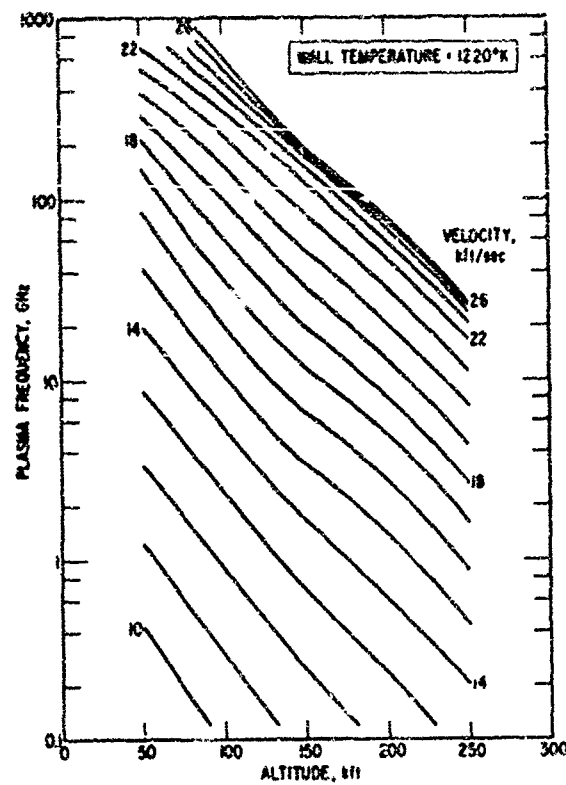


Fig. B-9. Maximum Plasma Frequency in Boundary Layer:  
Shock Angle = 50 deg

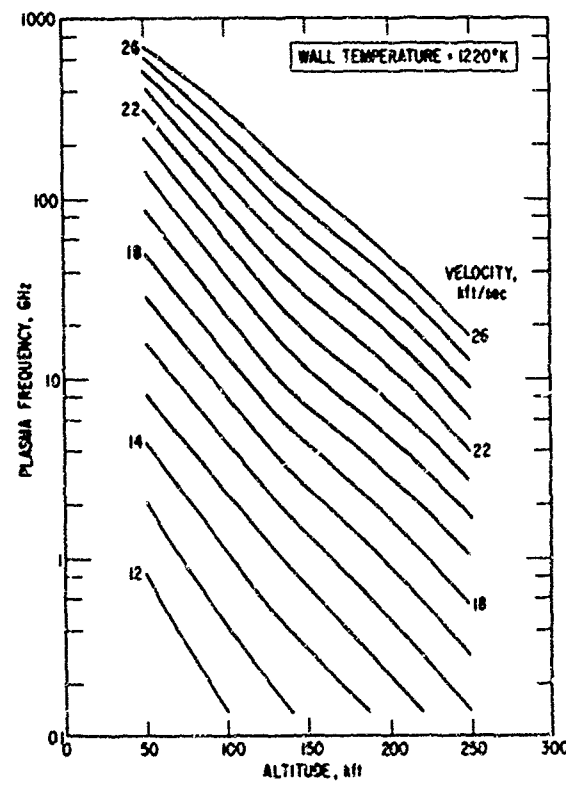


Fig. B-10. Maximum Plasma Frequency in Boundary Layer:  
Shock Angle = 40 deg

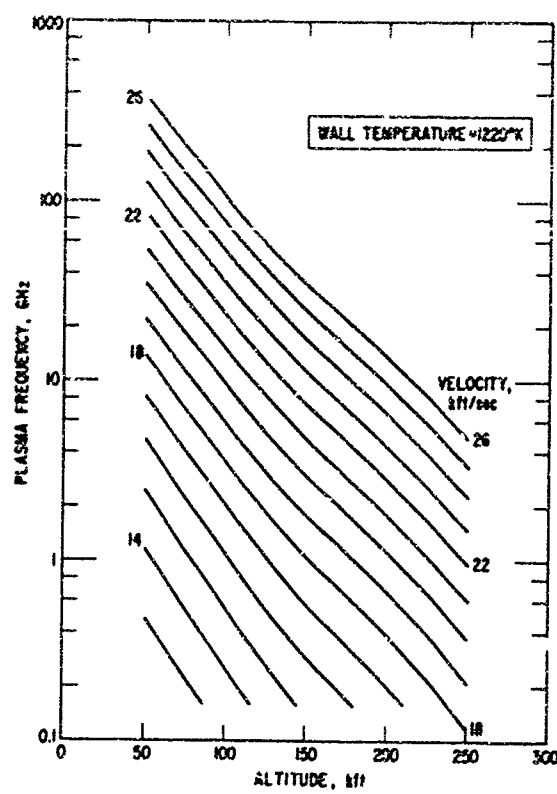


Fig. B-11. Maximum Plasma Frequency in Boundary Layer:  
Shock Angle = 30 deg

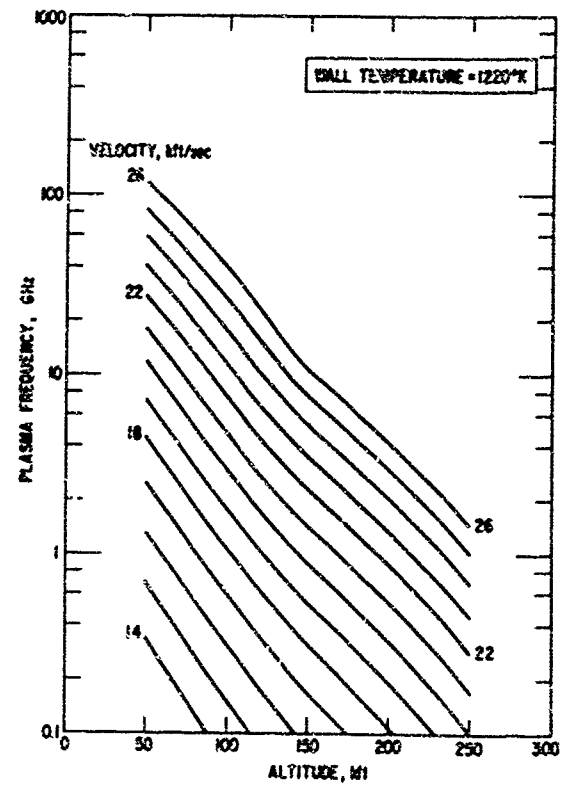


Fig. B-12. Maximum Plasma Frequency in Boundary Layer:  
Shock Angle = 20 deg

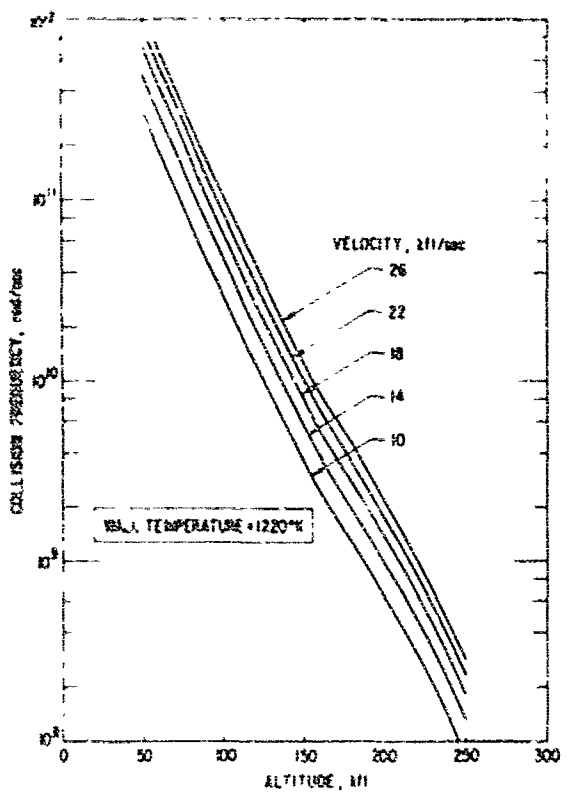


Fig. B-13. Collision Frequency at Peak Boundary Layer Condition: Shock Angle = 50 deg

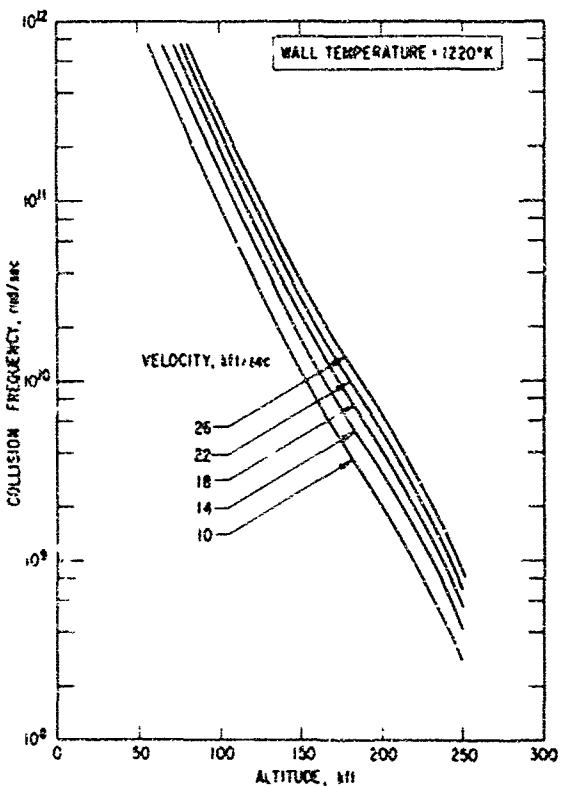


Fig. B-14. Collision Frequency at Peak Boundary Layer Condition: Shock Angle = 40 deg

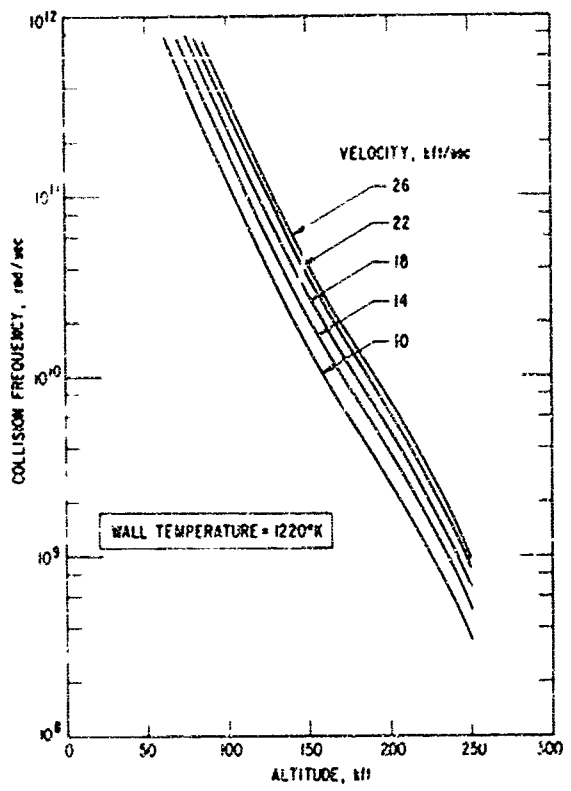


Fig. B-15. Collision Frequency at Peak Boundary Layer Condition: Shock Angle = 30 deg

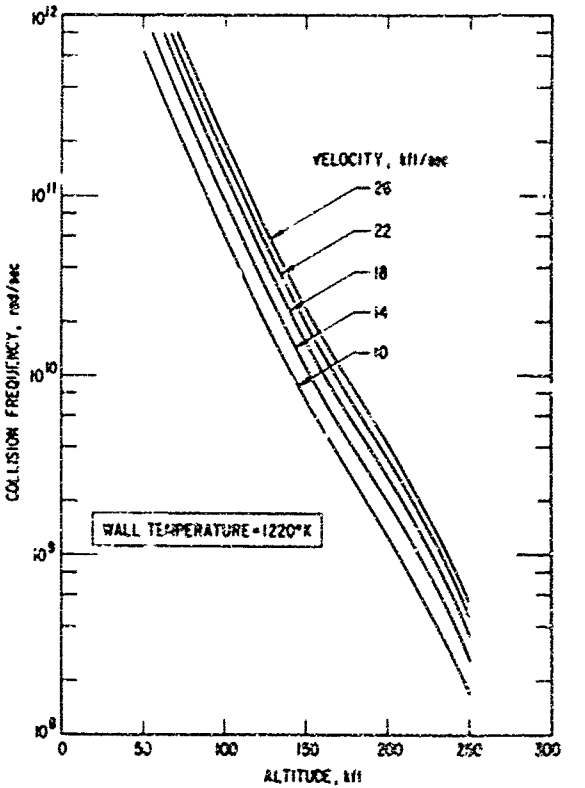


Fig. B-16. Collision Frequency at Peak Boundary Layer Condition: Shock Angle = 20 deg

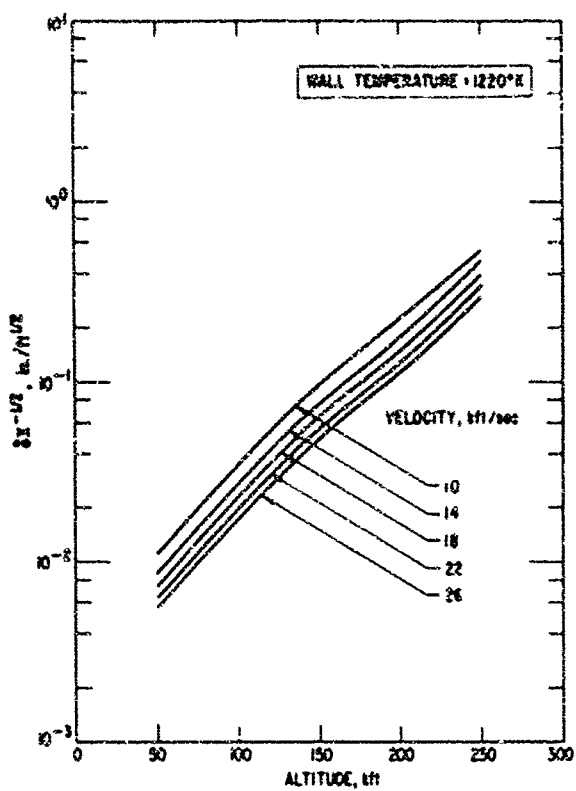


Fig. B-17. Wedge Boundary Layer Thickness (Laminar): Shock Angle = 50 deg

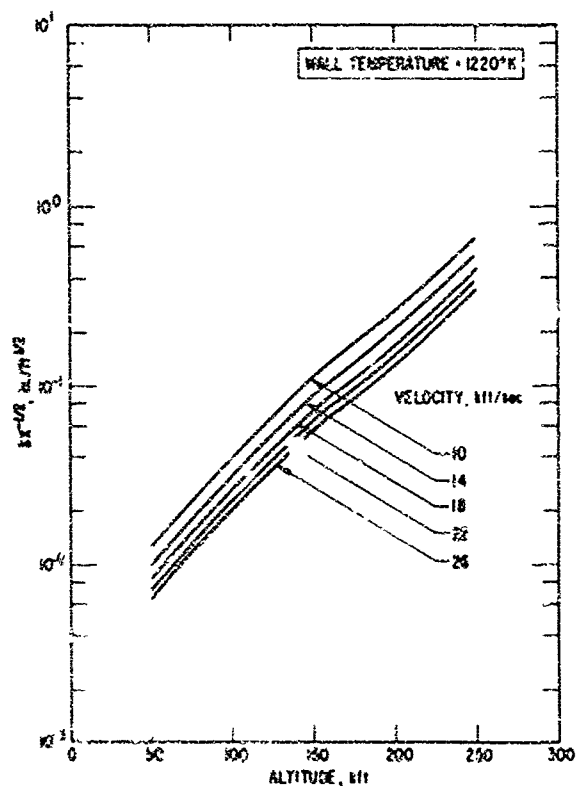


Fig. B-18. Wedge Boundary Layer Thickness (Laminar): Shock Angle = 40 deg

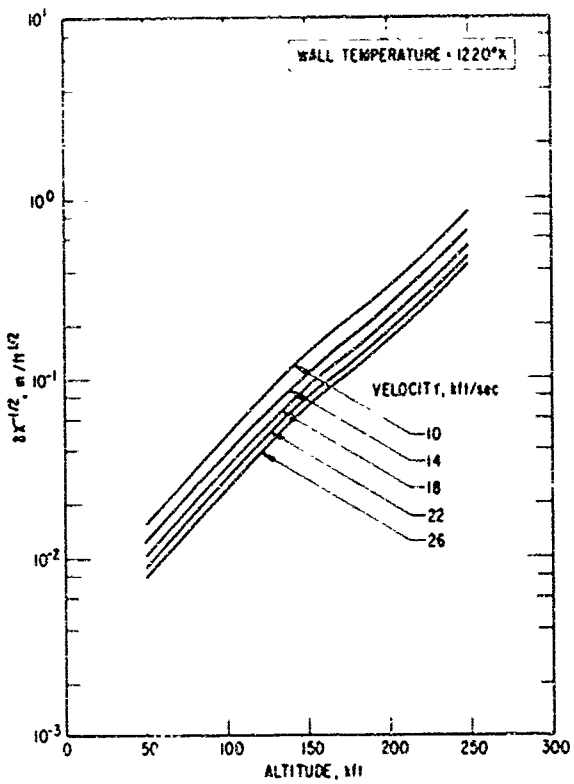


Fig. B-19. Wedge Boundary Layer Thickness (Laminar): Shock Angle = 30 deg

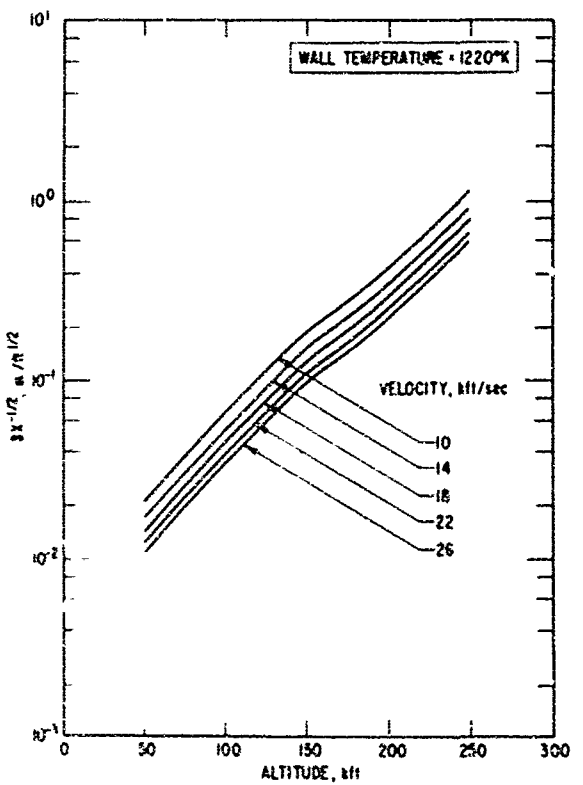


Fig. B-20. Wedge Boundary Layer Thickness (Laminar): Shock Angle = 20 deg

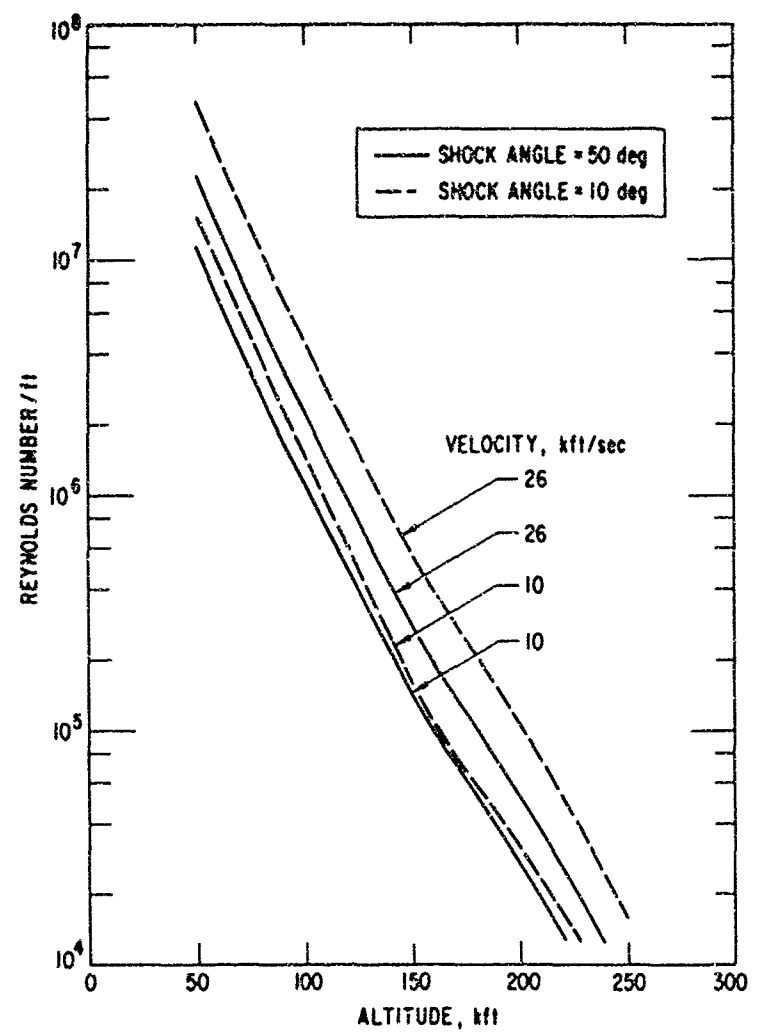


Fig. B-21. Boundary Layer Edge Reynolds Number (per foot) for Wedge

## REFERENCES

- B-1. Z. O. Bleviss, unpublished work.
- B-2. J. G. Logan, Jr., and L. E. Treanor, Tables of Thermodynamic Properties of Air from 3000°K to 10000°K at Intervals of 100°K, BE-1007-3-A, Cornell Aeronautical Lab., Inc., Buffalo, New York (January 1957).
- B-3. M. P. Bachynski, T. W. Johnston, and I. W. Shkarofsky, Electromagnetic Properties of High Temperature Air, Proc. IRE 48, 347 (1960).
- B-4. H. M. Musal, Jr., Plasma Frequency and Electron Collision Frequency Charts for Hypersonic Vehicle Equilibrium Flow Fields in Air, TR 62-209C, General Motors Corp. Defense Research Lab., Santa Barbara, Calif. (December 1962).
- B-5. C. E. Witliff and J. T. Curtis, Normal Shock Wave Parameters in Equilibrium Air, Rept. CAL-111, Cornell Aeronautical Lab., Inc., Buffalo, New York (November 1961).
- B-6. H. Serbin, "Supersonic Flow Around Blunt Bodies," J. Aerospace Sci. 25, 58-59 (1958).
- B-7. S. Feldman, Hypersonic Gas Dynamic Charts for Equilibrium Air, RR40, Avco-Everett Research Lab., Everett, Mass. (January 1957).
- B-8. M. F. Romig, Conical Flow Parameters for Air in Dissociation Equilibrium, RR7, Convair Scientific Research Lab., San Diego, Calif. (May 1960).

## APPENDIX C

## SIGNAL ATTENUATION

Signal attenuation calculated as indicated in Volume I, Section II-C-1, for cones, wedges, and stagnation points are presented in Tables C-I through C-XIII. The calculations were made for five signal frequencies (0.25, 0.5, 1.0, 5.0, 10 GHz) for representative points along both equilibrium glide and transient trajectories (see Volume I, Section II-A-1). Results are presented according to the following tabulation:

<u>Configuration</u>	<u>Body Station</u>	<u>Flow Field</u>	<u>Table</u>
Stag. Pt.	nose (3-in. radius)	Shock Layer	C-I
Sharp Wedge (50°)	{ 1 ft 5 ft	Shock Layer	C-II
Sharp Wedge (30°, 40°)	{ 1 ft 5 ft	{ Shock Layer Boundary Layer	C-III, V C-IV, VI
Sharp Wedge (20°)	{ 1 ft 5 ft	Boundary Layer	C-VII
Sharp Cone (50°)	{ 1 ft 5 ft	Shock Layer	C-VIII
Sharp Cone (30°, 40°)	{ 1 ft 5 ft	{ Shock Layer Boundary Layer	C-IX, XI C-X, XII
Sharp Cone (20°)	{ 1 ft 5 ft	Boundary Layer	C-XIII

Table C-XIV presents the characteristic incubation distance for electrons behind plane shock waves in air (Ref. C-1) compared with the appropriate shock layer thicknesses. These data have been used in the discussion of the importance of nonequilibrium effects in Volume I, Section II-C-2.

2 2 2 2 2 2 2	2 2 2 2 2 2 2	2 2 2 2 2 2 2	2 2 2 2 2 2 2
---------------	---------------	---------------	---------------

G.D

Table C-1. Stagnation Point Attenuation

Time, sec	Altitude, km	Velocity, km/sec	F <sub>p</sub> , GHz	n, rad/sec	d, fm	Alternation, dB					
						f = 250 MHz	f = 500 MHz	f = 1 GHz	f = 5 GHz	f = 10 GHz	
Trajectories											
0	308	25.6	6.5	$1.5 \times 10^8$	0.102	1.3	6.5	3.8	0.25	0.0	1
100	2.64	25.0	18.0	$1.2 \times 10^9$	0.111	2.9	26.0	22.5	7.8	2.0	1
150	2.47	24.0	28.0	$2.8 \times 10^9$	0.118	3.4	34.0	30.5	18.0	11.0	1
190	2.35	23.0	32.0	$4.0 \times 10^9$	0.123	3.4	35.0	35.0	22.0	15.0	1
230	2.27	22.0	35.0	$5.0 \times 10^9$	0.132	3.5	35.0	36.0	26.0	18.0	1
275	2.20	21.0	36.0	$5.5 \times 10^9$	0.136	3.4	36.0	35.0	28.0	22.0	1
320	2.14	20.0	37.0	$6.2 \times 10^9$	0.144	3.5	36.0	37.0	29.0	23.0	1
365	2.07	19.0	38.0	$7.0 \times 10^9$	0.153	3.5	36.0	38.0	32.0	25.0	1
0	300	25.6	6.5	$1.5 \times 10^8$	0.102	1.3	6.5	3.8	0.25	0.0	2
30	280	25.6	13.0	$5.5 \times 10^8$	0.105	2.6	20.0	14.0	3.3	1.2	2
60	26.9	25.6	25.0	$1.6 \times 10^9$	0.111	3.6	33.0	28.0	15.0	9.3	2
90	24.0	25.6	42.0	$4.4 \times 10^9$	0.117	3.9	40.0	40.0	28.0	24.0	2
120	22.0	25.6	65.0	$9.8 \times 10^9$	0.120	3.9	41.0	44.0	36.0	39.0	2
150	20.0	25.6	100.0	$2.0 \times 10^{10}$	0.123	4.2	44.0	47.0	62.0	60.0	2
170	20.0	25.0	95.0	$2.0 \times 10^9$	0.126	4.1	42.0	46.0	60.0	58.0	2
205	20.0	24.0	82.0	$1.8 \times 10^{10}$	0.129	4.2	40.0	44.0	55.0	53.0	2
240	20.0	23.0	75.0	$1.5 \times 10^{10}$	0.132	3.8	40.0	42.0	54.0	50.0	2
275	20.0	22.0	65.0	$1.5 \times 10^{10}$	0.136	3.6	37.0	40.0	43.0	41.0	2
305	20.0	21.0	58.0	$1.3 \times 10^{10}$	0.141	3.6	38.0	42.0	42.0	40.0	2
340	20.0	20.0	50.0	$1.1 \times 10^{10}$	0.147	3.5	38.0	40.0	40.0	35.0	2
375	20.0	19.0	43.0	$8.2 \times 10^9$	0.154	3.4	38.0	39.0	36.0	28.0	2
410	20.0	18.0	38.0	$8.1 \times 10^9$	0.162	3.5	36.0	38.0	34.0	27.0	1.2
450	19.4	17.0	37.0	$9.1 \times 10^8$	0.174	3.3	35.0	37.0	34.0	28.0	1.2
495	18.8	16.0	33.0	$9.0 \times 10^9$	0.183	3.1	32.0	34.0	30.0	24.0	1.2
540	18.2	15.0	22.0	$8.8 \times 10^9$	0.195	2.6	26.0	27.0	20.0	13.0	1.2
585	17.6	14.0	16.0	$9.0 \times 10^9$	0.201	2.0	20.0	21.0	13.0	7.0	1.2
625	17.0	13.0	8.0	$9.2 \times 10^9$	0.201	1.0	12.0	10.0	10.0	2.9	0.7
670	16.4	12.0	4.0	$9.2 \times 10^9$	0.207	4	3.8	3.2	0.1	0.1	0.1

Table C-II. Shock Layer Attenuation, 50-deg Wedge

Time, sec	Altitude, kft	Velocity, kit/sec	$f_p$ , GHz	$\nu_p$ , rad/sec	d(1 ft), in.	d(5 ft), in.	Attenuation, dB								Tracer 1 v Equil. 2 v Trans.	
							$f = 250$ MHz		$f = 500$ MHz		$f = 1$ GHz		$f = 5$ GHz		$f = 10$ GHz	
							1 ft	5 ft	1 ft	5 ft	1 ft	5 ft	1 ft	5 ft	1 ft	5 ft
0	300	25.6	$3.4 \times 10^7$	1.04	5.22	26.0	91	21.0	85	14.0	71	0.4	0.1	0.0	0.0	1
100	266	25.0	$10.0 \times 10^6$	1.09	5.44	63.0	Large	42.0	261	57.0	257	38.0	212.0	10.0	27.0	1
150	247	24.0	$17.0 \times 10^6$	1.17	5.85	97.0	Large	96.0	Large	95.0	46.6	77.0	440.0	63.0	366.0	1
190	236	23.0	$20.0 \times 10^6$	1.19	5.95	100.0	Large	104.0	Large	118.0	54	105.0	Large	90.0	472.0	1
210	227	22.0	$22.0 \times 10^6$	1.28	6.38	102.0	Large	123.0	Large	130.0	60.4	128.0	Large	103.0	572.0	1
275	220	21.0	$3.2 \times 10^9$	1.34	6.70	100.0	Large	126.0	Large	139.0	64.3	136.0	Large	110.0	604.0	1
320	214	20.0	$21.0 \times 10^9$	1.38	6.90	91.0	Large	117.0	Large	133.0	60.9	131.0	Large	105.0	561.0	1
365	207	19.0	$20.5 \times 10^9$	1.46	7.31	88.0	Large	114.0	Large	133.0	61.1	139.0	Large	112.0	589.0	1
0	300	25.6	$3.4 \times 10^7$	1.04	5.22	26.0	91	21.0	85	7.7	711	0.4	0.5	0.0	<1	2
30	280	25.6	$6.9 \times 10^8$	1.04	5.22	50.0	182	46.0	175	37.0	169	18.0	128.0	0.4	1.0	2
60	260	25.6	$9.8 \times 10^8$	1.04	5.22	80.0	Large	79.0	Large	70.0	529	57.0	298.0	38.0	232.0	2
90	248	25.6	$22.2 \times 10^9$	1.04	5.42	94.0	Large	106.0	Large	118.0	518	104.0	498.0	80.0	471.0	2
120	220	25.6	$35.0 \times 10^9$	1.04	5.22	117.5	Large	148.0	Large	168.0	Large	171.0	Large	159.0	Large	2
150	200	25.6	$6.2 \times 10^{10}$	1.04	5.22	100.0	Large	331.0	Large	385.0	Large	260.0	Large	270.0	Large	2
170	200	25.0	$55.0 \times 10^{10}$	1.09	5.44	100.0	Large	133.3	Large	181.0	Large	253.0	Large	233.0	Large	2
205	200	24.0	$50.0 \times 10^{10}$	1.17	5.89	105.0	Large	138.0	Large	192.0	Large	248.0	Large	265.0	Large	2
240	200	23.0	$45.0 \times 10^{10}$	1.19	5.95	102.0	Large	134.0	Large	184.0	Large	243.0	Large	246.0	Large	2
275	200	22.0	$40.0 \times 10^{10}$	1.28	6.38	103.0	Large	139.0	Large	186.0	Large	230.0	Large	232.0	Large	2
305	205	21.0	$34.0 \times 10^{10}$	1.34	6.70	98.0	Large	125.0	Large	184.0	Large	200.0	Large	206.0	Large	2
340	200	20.0	$6.5 \times 10^9$	1.38	6.90	83.0	Large	119.0	Large	160.0	Large	180.0	Large	170.0	Large	2
375	200	19.0	$22.0 \times 10^9$	1.46	7.31	80.0	Large	113.0	Large	133.0	61.2	150.0	Large	128.0	Large	2
410	200	18.0	$18.0 \times 10^9$	1.46	7.31	75.0	Large	97.0	Large	123.0	519	115.0	Large	96.0	494.0	1.2
450	194	17.0	$14.5 \times 10^9$	1.54	7.72	62.0	236	78.0	Large	93.0	423	94.0	Large	69.0	343.0	1.2
495	188	16.0	$9.0 \times 10^9$	1.63	8.25	43.0	159	53.0	223	51.0	281	52.0	275.0	7.9	81.0	1.2
540	182	15.0	$5.5 \times 10^9$	1.74	8.88	28.0	101	34.0	138	39.0	180	17.0	82.0	1.4	<10	1.2
585	176	14.0	$3.3 \times 10^9$	1.99	9.30	17.9	61	19.0	83	22.0	105	2.4	12.3	0.5	<10	1.2
625	170	13.0	$2.2 \times 10^9$	2.06	10.30	11.0	43	12.0	97	12.0	64	1.1	<10	0.2	<10	1.2
670	164	12.0	$1.6 \times 10^9$	2.29	11.40	7.5	30	6.0	38	5.2	31	0.6	<10	0.6	<10	1.2

Table C-III. Shock Layer Attenuation, 40-deg Wedge

Time sec	Altitude, km	Velocity, km/sec	$\frac{V}{c}$ , GHz	$\frac{V}{c}$ , rad/sec	Attenuation, dB										Transit time sec	
					0.00	0.50	1.00	1.50	2.00	2.50	3.00	3.50	4.00	5.00		
0	100	25.6	2.2	$5.9 \times 10^7$	0.90	4.90	16.0	32	10.0	49.0	4.0	33.0	6.0	6.0	0.0	
100	264	25.0	6.0	$4.1 \times 10^8$	0.90	4.90	45.0	160	35.0	150.0	15.0	222.0	32.0	11.0	6.7	
150	247	24.0	10.5	$9.3 \times 10^8$	0.94	4.71	61.0	224	50.0	235.0	30.0	184.0	11.0	44.0	1	
170	236	23.0	12.0	$1.4 \times 10^9$	0.90	4.92	62.0	231	65.0	263.0	45.0	277.0	66.0	26.0	135.0	
230	227	22.0	12.0	$1.0 \times 10^9$	1.04	5.24	61.0	222	62.0	264.0	65.0	270.0	53.0	27.0	143.0	
275	220	21.0	11.0	$2.1 \times 10^9$	1.04	5.22	57.0	210	55.0	212.0	61.0	265.0	50.0	27.0	143.0	
320	214	20.0	9.5	$4.4 \times 10^9$	1.07	5.14	49.0	134	42.0	173.0	54.0	234.0	35.0	17.0	12.0	
365	207	19.0	7.0	$3.0 \times 10^9$	1.13	5.65	31.0	160	41.0	164.0	60.0	179.0	25.0	119.0	0.5	
0	300	25.6	2.2	$5.9 \times 10^7$	0.90	4.90	16.0	52	10.0	49.0	4.0	33.0	6.0	6.0	0.0	2
30	260	25.6	6.0	$4.0 \times 10^8$	0.90	4.90	35.0	111	27.0	107.0	7.0	97.0	2.0	3.1	0.0	2
60	260	25.6	9.0	$6.2 \times 10^8$	0.90	4.90	55.0	269	51.0	206.0	46.0	282.0	27.0	150.0	2.0	3.2
90	240	25.6	15.0	$1.5 \times 10^9$	0.90	4.90	73.0	276	77.0	318.0	76.0	333.0	69.0	291.0	42.0	170.0
120	220	25.6	26.0	$3.3 \times 10^9$	0.90	4.90	87.0	365	101.0	Large	100.0	450.0	160.0	460.0	95.0	370.0
150	200	25.6	37.0	$7.0 \times 10^9$	0.90	4.90	90.0	365	130.0	Large	150.0	520.0	165.0	Large	151.0	Large
170	200	25.0	34.0	$7.0 \times 10^9$	0.90	4.90	74.0	360	101.0	Large	145.0	610.0	154.0	600.0	163.0	600.0
205	200	24.0	30.0	$2.1 \times 10^9$	0.94	6.71	130.0	Large	124.0	Large	144.0	650.0	132.0	650.0	121.0	615.0
240	200	23.0	26.0	$6.0 \times 10^9$	0.90	4.92	64.0	234	81.0	122.0	103.0	490.0	107.0	550.0	96.0	530.0
275	200	22.0	20.0	$5.1 \times 10^9$	1.04	5.22	61.0	420	65.0	245.0	95.0	415.0	93.0	440.0	60.0	430.0
305	200	21.0	19.5	$4.0 \times 10^9$	1.04	5.22	49.0	173	59.0	235.0	72.0	317.0	67.0	330.0	52.0	215.0
340	200	20.0	12.0	$4.1 \times 10^9$	1.07	5.14	41.0	134	54.0	226.0	63.0	275.0	53.0	271.0	24.5	110.0
375	200	19.0	8.0	$3.0 \times 10^9$	1.13	5.65	35.0	114	43.0	164.0	43.0	197.0	29.0	160.0	3.4	20.0
410	200	18.0	5.00	$3.1 \times 10^9$	1.17	5.05	19.0	73	28.0	112.0	17.0	125.0	7.0	31.0	0.0	0.5
450	192	17.0	3.20	$3.4 \times 10^9$	1.20	6.28	16.0	44	17.0	65.0	13.0	67.0	1.0	4.0	0.0	1.2
495	184	16.0	1.80	$3.9 \times 10^9$	1.36	6.80	10.0	33	9.0	42.0	5.0	40.0	0.2	1.0	0.0	1.2
540	182	15.0	1.70	$4.5 \times 10^9$	1.44	7.23	5.0	19	5.0	27.0	2.5	22.0	0.1	0.6	0.0	1.2
585	176	14.0	0.65	$4.1 \times 10^9$	1.44	7.20	2.0	10	2.4	16.0	1.0	9.5	0.1	0.2	0.0	1.2
625	170	13.0	0.65	$4.5 \times 10^9$	1.54	7.72	1.5	7	1.4	8.5	0.4	4.2	0.0	0.2	0.0	1.2
670	164	12.0	0.40	$4.0 \times 10^9$	1.67	8.35	1.0	5	0.8	4.0	0.3	2.5	0.0	0.1	0.0	1.2

Table C-IV. Boundary Layer Attenuation, 40-deg Wedge

Time, sec	Altitude, ft	Velocity, ft/sec	$\frac{t_p}{\text{hrs}}$	Radius, in.	dln. in.	Attenuation						Trans.
						$\frac{1}{\text{in}} \cdot 10^4$						
0	360	25.6	-	-	-	-	-	-	-	-	-	-
100	46.6	25.0	-	-	-	-	-	-	-	-	-	-
150	24.7	24.0	16.0	$9.8 \times 10^3$	0.31	0.70	44.0	71.0	40.0	67.0	34.0	45.0
190	19.6	19.0	16.5	$1.5 \times 10^3$	0.26	0.58	35.0	52.0	31.0	53.0	32.0	36.0
230	22.7	22.0	15.5	$2.1 \times 10^3$	0.22	0.50	30.0	48.0	29.0	45.0	36.0	31.0
270	27.9	21.0	16.0	$2.6 \times 10^3$	0.21	0.46	21.0	29.0	21.0	29.0	21.0	27.0
320	21.4	20.0	7.4	$3.2 \times 10^3$	0.19	0.42	16.0	23.0	16.0	20.0	17.0	17.0
360	20.7	19.0	9.6	$3.9 \times 10^3$	0.17	0.34	10.0	14.0	8.0	12.0	6.0	6.0
400	20.0	19.6	-	-	-	-	-	-	-	-	-	-
450	19.0	19.6	-	-	-	-	-	-	-	-	-	-
500	14.0	20.0	25.6	-	-	-	-	-	-	-	-	-
540	9.0	25.0	25.6	-	-	-	-	-	-	-	-	-
580	4.0	25.0	25.6	-	-	-	-	-	-	-	-	-
620	22.0	25.0	25.6	-	-	-	-	-	-	-	-	-
660	19.0	25.0	25.6	-	-	-	-	-	-	-	-	-
700	14.0	25.0	25.6	-	-	-	-	-	-	-	-	-
740	9.0	25.0	25.6	-	-	-	-	-	-	-	-	-
780	4.0	25.0	25.6	-	-	-	-	-	-	-	-	-
820	22.0	25.0	25.6	-	-	-	-	-	-	-	-	-
860	19.0	25.0	25.6	-	-	-	-	-	-	-	-	-
900	14.0	25.0	25.6	-	-	-	-	-	-	-	-	-
940	9.0	25.0	25.6	-	-	-	-	-	-	-	-	-
980	4.0	25.0	25.6	-	-	-	-	-	-	-	-	-
1020	22.0	25.0	25.6	-	-	-	-	-	-	-	-	-
1060	19.0	25.0	25.6	-	-	-	-	-	-	-	-	-
1100	14.0	25.0	25.6	-	-	-	-	-	-	-	-	-
1140	9.0	25.0	25.6	-	-	-	-	-	-	-	-	-
1180	4.0	25.0	25.6	-	-	-	-	-	-	-	-	-
1220	22.0	25.0	25.6	-	-	-	-	-	-	-	-	-
1260	19.0	25.0	25.6	-	-	-	-	-	-	-	-	-
1300	14.0	25.0	25.6	-	-	-	-	-	-	-	-	-
1340	9.0	25.0	25.6	-	-	-	-	-	-	-	-	-
1380	4.0	25.0	25.6	-	-	-	-	-	-	-	-	-
1420	22.0	25.0	25.6	-	-	-	-	-	-	-	-	-
1460	19.0	25.0	25.6	-	-	-	-	-	-	-	-	-
1500	14.0	25.0	25.6	-	-	-	-	-	-	-	-	-
1540	9.0	25.0	25.6	-	-	-	-	-	-	-	-	-
1580	4.0	25.0	25.6	-	-	-	-	-	-	-	-	-
1620	22.0	25.0	25.6	-	-	-	-	-	-	-	-	-
1660	19.0	25.0	25.6	-	-	-	-	-	-	-	-	-
1700	14.0	25.0	25.6	-	-	-	-	-	-	-	-	-
1740	9.0	25.0	25.6	-	-	-	-	-	-	-	-	-
1780	4.0	25.0	25.6	-	-	-	-	-	-	-	-	-
1820	22.0	25.0	25.6	-	-	-	-	-	-	-	-	-
1860	19.0	25.0	25.6	-	-	-	-	-	-	-	-	-
1900	14.0	25.0	25.6	-	-	-	-	-	-	-	-	-
1940	9.0	25.0	25.6	-	-	-	-	-	-	-	-	-
1980	4.0	25.0	25.6	-	-	-	-	-	-	-	-	-
2020	22.0	25.0	25.6	-	-	-	-	-	-	-	-	-
2060	19.0	25.0	25.6	-	-	-	-	-	-	-	-	-
2100	14.0	25.0	25.6	-	-	-	-	-	-	-	-	-
2140	9.0	25.0	25.6	-	-	-	-	-	-	-	-	-
2180	4.0	25.0	25.6	-	-	-	-	-	-	-	-	-
2220	22.0	25.0	25.6	-	-	-	-	-	-	-	-	-
2260	19.0	25.0	25.6	-	-	-	-	-	-	-	-	-
2300	14.0	25.0	25.6	-	-	-	-	-	-	-	-	-
2340	9.0	25.0	25.6	-	-	-	-	-	-	-	-	-
2380	4.0	25.0	25.6	-	-	-	-	-	-	-	-	-
2420	22.0	25.0	25.6	-	-	-	-	-	-	-	-	-
2460	19.0	25.0	25.6	-	-	-	-	-	-	-	-	-
2500	14.0	25.0	25.6	-	-	-	-	-	-	-	-	-
2540	9.0	25.0	25.6	-	-	-	-	-	-	-	-	-
2580	4.0	25.0	25.6	-	-	-	-	-	-	-	-	-
2620	22.0	25.0	25.6	-	-	-	-	-	-	-	-	-
2660	19.0	25.0	25.6	-	-	-	-	-	-	-	-	-
2700	14.0	25.0	25.6	-	-	-	-	-	-	-	-	-
2740	9.0	25.0	25.6	-	-	-	-	-	-	-	-	-
2780	4.0	25.0	25.6	-	-	-	-	-	-	-	-	-
2820	22.0	25.0	25.6	-	-	-	-	-	-	-	-	-
2860	19.0	25.0	25.6	-	-	-	-	-	-	-	-	-
2900	14.0	25.0	25.6	-	-	-	-	-	-	-	-	-
2940	9.0	25.0	25.6	-	-	-	-	-	-	-	-	-
2980	4.0	25.0	25.6	-	-	-	-	-	-	-	-	-
3020	22.0	25.0	25.6	-	-	-	-	-	-	-	-	-
3060	19.0	25.0	25.6	-	-	-	-	-	-	-	-	-
3100	14.0	25.0	25.6	-	-	-	-	-	-	-	-	-
3140	9.0	25.0	25.6	-	-	-	-	-	-	-	-	-
3180	4.0	25.0	25.6	-	-	-	-	-	-	-	-	-
3220	22.0	25.0	25.6	-	-	-	-	-	-	-	-	-
3260	19.0	25.0	25.6	-	-	-	-	-	-	-	-	-
3300	14.0	25.0	25.6	-	-	-	-	-	-	-	-	-
3340	9.0	25.0	25.6	-	-	-	-	-	-	-	-	-
3380	4.0	25.0	25.6	-	-	-	-	-	-	-	-	-
3420	22.0	25.0	25.6	-	-	-	-	-	-	-	-	-
3460	19.0	25.0	25.6	-	-	-	-	-	-	-	-	-
3500	14.0	25.0	25.6	-	-	-	-	-	-	-	-	-
3540	9.0	25.0	25.6	-	-	-	-	-	-	-	-	-
3580	4.0	25.0	25.6	-	-	-	-	-	-	-	-	-
3620	22.0	25.0	25.6	-	-	-	-	-	-	-	-	-
3660	19.0	25.0	25.6	-	-	-	-	-	-	-	-	-
3700	14.0	25.0	25.6	-	-	-	-	-	-	-	-	-
3740	9.0	25.0	25.6	-	-	-	-	-	-	-	-	-
3780	4.0	25.0	25.6	-	-	-	-	-	-	-	-	-
3820	22.0	25.0	25.6	-	-	-	-	-	-	-	-	-
3860	19.0	25.0	25.6	-	-	-	-	-	-	-	-	-
3900	14.0	25.0	25.6	-	-	-	-	-	-	-	-	-
3940	9.0	25.0	25.6	-	-	-	-	-	-	-	-	-
3980	4.0	25.0	25.6	-	-	-	-	-	-	-	-	-
4020	22.0	25.0	25.6	-	-	-	-	-	-	-	-	-
4060	19.0	25.0	25.6	-	-	-	-	-	-	-	-	-
4100	14.0	25.0	25.6	-	-	-	-	-	-	-	-	-
4140	9.0	25.0	25.6	-	-	-	-	-	-	-	-	-
4180	4.0	25.0	25.6	-	-	-	-	-	-	-	-	-
4220	22.0	25.0	25.6	-	-	-	-	-	-	-	-	-
4260	19.0	25.0	25.6	-	-	-	-	-	-	-	-	-
4300	14.0	25.0	25.6	-	-	-	-	-	-	-	-	-
4340	9.0	25.0	25.6	-	-	-	-	-	-	-	-	-
4380	4.0	25.0	25.6	-	-	-	-	-	-	-	-	-
4420	22.0	25.0	25.6	-	-	-	-	-	-	-	-	-
4460	19.0	25.0	25.6	-	-	-	-	-	-	-	-	-
4500	14.0	25.0	25.6	-	-	-	-	-	-	-	-	-
4540	9.0	25.0	25.6	-	-	-	-	-	-	-	-	-
4580	4.0	25.0	25.6	-	-	-	-	-	-	-	-	-
4620	22.0	25.0	25.6	-	-	-	-	-	-	-	-	-
4660	19.0	25.0	25.6	-	-	-	-	-	-	-	-	-
4700	14.0	25.0	25.6	-	-	-	-	-	-	-	-	-
4740	9.0	25.0	25.6	-	-	-	-	-	-	-	-	-
4780	4.0	25.0	25.6	-	-	-	-	-	-	-	-	-
4820	22.0	25.0	25.6	-	-	-	-	-	-	-	-	-
4860	19.0	25.0	25.6</									

Table C-V. Shock Layer Attenuation, 30-deg Wedge

Time, sec	Altitude, km	Velocity, km/sec	$f_p$ , GHz	$\nu$ , rad/sec	$d(f_m)$ , in	$d(f_m)$ , in	Attenuation, dB								Project 1 = Aquit. 2 = Trans.	
							$f = 2500$ MHz		$f = 5000$ MHz		$f = 10$ GHz		$f = 5$ GHz			
							$f_m$	$S_m$	$f_m$	$S_m$	$f_m$	$S_m$	$f_m$	$S_m$		
0	300	25.6	0.90	$3.0 \times 10^7$	0.73	3.66	1.5	13.0	0.45	7.5	0.10	1.8	0.0	0.0	0.0	
100	266	25.0	2.00	$2.1 \times 10^8$	0.73	3.66	10.7	38.5	6.00	32.0	2.70	24.5	0.0	0.0	0.0	
150	247	24.0	2.40	$5.6 \times 10^8$	0.75	3.77	13.5	49.0	8.60	40.0	6.06	39.0	0.1	0.2	0.0	
190	235	23.0	2.00	$8.0 \times 10^8$	0.80	3.96	10.7	40.0	6.40	37.3	3.00	25.5	0.0	0.0	0.0	
230	227	22.0	1.50	$1.1 \times 10^9$	0.84	4.16	5.4	28.0	4.60	24.3	1.70	14.5	0.0	0.0	0.0	
275	220	21.0	0.95	$1.3 \times 10^9$	0.86	4.30	5.8	17.0	1.40	11.0	0.50	4.5	0.0	0.0	0.0	
320	214	20.0	0.66	$1.4 \times 10^9$	0.92	4.60	2.1	10.0	0.83	6.2	0.25	1.5	0.0	0.0	0.0	
365	207	19.0	0.60	$1.7 \times 10^9$	0.96	4.80	1.7	8.4	0.55	3.5	0.20	1.5	0.0	0.0	0.0	
410	200	25.6	0.9	$3.0 \times 10^7$	0.73	3.66	1.3	13.0	0.45	7.5	0.10	1.7	0.0	0.0	0.0	
450	192	25.6	1.6	$1.0 \times 10^8$	0.73	3.66	7.5	57.5	3.40	26.00	1.10	15.5	0.1	0.2	0.0	
495	184	25.6	3.0	$3.2 \times 10^8$	0.73	3.66	19.0	60.0	12.50	52.00	7.80	46.0	0.2	0.4	0.0	
540	182	25.6	5.0	$9.0 \times 10^8$	0.75	3.66	28.0	95.0	23.50	37.00	16.50	85.0	3.0	14.5	0.0	
585	176	25.6	7.9	$1.9 \times 10^9$	0.73	3.66	37.0	113.0	33.50	125.00	32.00	135.0	20.0	98.0	1.5	
625	170	25.0	11.0	$4.0 \times 10^9$	0.73	3.66	39.0	123.0	40.00	147.00	41.00	73.0	29.0	160.0	1.0	
670	164	22.0	19.0	0.7	$2.2 \times 10^9$	0.96	4.80	1.10	6.80	0.40	2.6	0.0	0.0	0.0	0.0	
715	200	23.0	4.5	$3.1 \times 10^9$	0.80	3.98	22.5	71.5	23.00	79.50	22.00	94.0	6.0	40.0	4.0	
755	200	22.0	3.0	$3.0 \times 10^9$	0.84	4.18	13.8	42.0	12.00	47.00	9.50	48.0	0.2	0.3	0.0	
805	200	21.0	1.7	$2.6 \times 10^9$	0.86	4.30	8.0	22.5	5.50	24.00	2.90	21.5	0.1	0.1	0.0	
840	200	20.0	1.0	$2.3 \times 10^9$	0.92	4.60	3.0	12.0	2.20	13.00	0.85	7.0	0.0	0.0	0.0	
875	200	19.0	0.7	$2.2 \times 10^9$	0.96	4.80	1.5	7.0	1.10	6.80	0.40	2.6	0.0	0.0	0.0	
910	200	18.0	0.50	$2.0 \times 10^9$	0.96	4.80	1.10	5.60	0.5	3.2	0.2	0.90	0.0	0.0	0.0	
950	192	17.0	0.40	$2.2 \times 10^9$	0.98	4.92	0.45	2.40	0.3	1.9	0.1	0.50	0.0	0.0	0.0	
995	184	16.0	0.31	$2.2 \times 10^9$	1.07	5.34	0.35	2.00	0.2	1.2	0.1	0.35	0.0	0.0	0.0	
1040	182	15.0	0.20	$2.2 \times 10^9$	1.15	5.75	0.10	1.00	0.1	0.5	0.0	0.20	0.0	0.0	0.0	
1085	176	14.0	0.13	$2.5 \times 10^9$	1.21	6.05	0.10	0.30	0.0	0.2	0.0	0.10	0.0	0.0	0.0	
1130	170	13.0	0.08	$2.5 \times 10^9$	1.32	6.58	0.00	0.25	0.0	0.1	0.0	0.00	0.0	0.0	0.0	
1170	164	12.0	-	-	-	-	-	-	-	-	-	-	-	-	-	

Table C-VI. Boundary Layer Attenuation, 30-deg Wedge

Table C-VII. Boundary Layer Attenuation, 20-deg Wedge

Time, sec	Altitude, mi	Velocity, mi/sec	$\frac{1}{\rho}$ , Ghz	$\nu$ , rad/sec	distn., in.	distn., in.	Attenuation, dB						Trans. 1 = Equil. 2 = Trans.
							1 = 250 MHz 1/10	1 = 500 MHz 1/10	1 = 1 GHz 1/10	1 = 5 GHz 1/10	1 = 10 GHz 1/10	1 = 10 GHz 1/10	
0	300	25.6	-	-	-	-	-	-	-	-	-	-	-
100	26.6	25.0	-	-	-	-	-	-	-	-	-	-	-
150	24.7	24.0	1.010	$3.7 \times 10^8$	0.50	1.10	1.7	4.0	6.5	1.4	0.2	0.4	-
190	23.6	23.0	0.860	$6.2 \times 10^8$	0.40	0.91	1.2	3.5	6.4	1.1	0.1	0.3	-
230	22.7	22.0	0.710	$8.5 \times 10^8$	0.34	0.80	0.7	2.0	6.4	0.5	0.0	0.1	-
275	22.0	21.0	0.580	$1.1 \times 10^9$	0.32	0.72	0.3	1.1	6.1	0.3	0.0	0.1	-
320	21.4	20.0	0.375	$1.3 \times 10^9$	0.30	0.66	0.2	0.4	6.1	0.2	0.0	0.1	-
365	20.7	19.0	0.265	$1.5 \times 10^9$	0.26	0.59	0.1	0.2	6.0	0.1	0.0	0.0	-
410	20.0	18.0	0.182	$1.9 \times 10^9$	0.24	0.54	0.0	0.1	6.0	0.0	0.0	0.0	-
450	19.4	17.0	-	-	-	-	-	-	-	-	-	-	-
495	18.6	16.0	-	-	-	-	-	-	-	-	-	-	-
540	18.2	15.0	-	-	-	-	-	-	-	-	-	-	-
585	17.6	14.0	-	-	-	-	-	-	-	-	-	-	-
625	17.0	13.0	-	-	-	-	-	-	-	-	-	-	-
670	16.4	12.0	-	-	-	-	-	-	-	-	-	-	-

Table C-VIII. Shock Layer Attenuation, 50-deg Cone

Time, sec	Altitude, kft	Velocity, kft/sec	$\frac{f}{P}$ , GHz	d1 (ft), in.	d2 (ft), in.	d3 (ft), in.	Attenuation, dB						Project. Eqw.	2, Trans.	
							$f = 250$ MHz	$f = 500$ MHz	$f = 1$ GHz	$f = 5$ GHz	$f = 10$ GHz				
0	100	23.6	2.9	$7.5 \times 10^7$	0.52	2.62	14.0	44.0	38.0	4.2	29.0	0.2	0.1	0.1	
100	26.0	25.0	9.2	$6.0 \times 10^8$	0.54	2.72	41.0	130.0	35.0	137.0	122.0	14.0	92.0	3.0	
150	24.7	24.0	15.5	$1.4 \times 10^9$	0.58	2.92	57.0	186.0	57.0	216.0	53.0	219.0	38.0	198.0	1.0
190	23.6	23.0	18.0	$2.0 \times 10^9$	0.58	2.92	59.0	211.0	62.0	235.0	60.0	249.0	47.0	234.0	0.0
230	22.7	22.0	19.5	$2.6 \times 10^9$	0.58	2.92	57.0	190.0	63.0	239.0	64.0	263.0	51.0	256.0	199.0
275	22.0	21.0	18.0	$2.7 \times 10^9$	0.49	3.25	57.0	199.0	63.0	239.0	64.0	267.0	52.0	257.0	223.0
320	21.4	20.0	18.0	$3.2 \times 10^9$	0.71	3.56	55.0	188.0	61.0	247.0	67.0	263.0	56.0	272.0	220.0
365	20.7	19.0	17.0	$4.0 \times 10^9$	0.73	3.66	49.0	167.0	58.0	225.0	62.0	249.0	54.0	273.0	227.0
400	25.6	25.6	4.9	$7.5 \times 10^7$	0.52	2.62	14.0	44.0	5.0	39.0	4.2	29.0	0.2	0.1	0.1
50	28.0	25.6	6.2	$2.7 \times 10^8$	0.52	2.62	30.0	91.0	26.0	84.0	10.0	77.0	4.3	39.0	0.4
60	26.0	23.6	12.0	$9.0 \times 10^8$	0.58	2.62	47.0	182.0	47.0	155.0	38.0	192.0	23.0	13.0	0.4
90	24.0	23.6	20.5	$2.2 \times 10^9$	0.52	2.62	58.0	198.0	62.0	232.0	64.0	247.0	49.0	14.0	210.0
120	22.9	23.4	33.0	$5.0 \times 10^9$	0.52	2.62	61.0	283.0	74.0	294.0	81.0	348.0	74.0	374.0	2
150	20.9	21.6	52.0	$1.1 \times 10^{10}$	0.52	2.62	62.0	287.0	76.0	289.0	98.0	495.0	129.0	124.0	Large
170	20.0	20.9	56.0	$1.6 \times 10^{10}$	0.54	2.72	62.0	210.0	77.0	289.0	97.0	419.0	126.0	421.0	Large
200	20.0	20.0	44.0	$9.5 \times 10^8$	0.58	2.92	62.0	210.0	77.0	293.0	98.0	422.0	122.0	583.0	2
230	20.0	21.9	40.0	$6.2 \times 10^9$	0.58	2.92	62.0	210.0	77.0	293.0	94.0	407.0	111.0	334.0	2
275	20.0	24.0	34.0	$7.2 \times 10^9$	0.58	2.92	61.0	172.0	76.0	265.0	66.0	345.0	95.0	444.0	2
300	20.0	21.0	36.0	$6.5 \times 10^9$	0.64	3.25	58.0	196.0	76.0	286.0	66.0	362.0	91.0	443.0	2
340	20.0	20.0	25.0	$3.7 \times 10^9$	0.71	3.56	54.0	192.0	69.0	243.0	79.0	317.0	82.0	397.0	2
375	20.0	19.0	16.0	$5.0 \times 10^9$	0.73	3.66	47.0	197.0	56.0	219.0	63.0	346.0	58.0	288.0	247.0
410	20.0	18.0	14.0	$4.2 \times 10^9$	0.75	3.75	42.0	139.0	59.0	188.0	53.0	223.0	43.0	233.0	165.0
450	19.4	17.0	9.5	$5.0 \times 10^9$	0.80	3.98	31.0	92.0	35.0	135.0	34.0	159.0	25.0	142.0	0.2
495	18.8	16.0	6.0	$5.0 \times 10^9$	0.86	4.29	22.0	64.0	23.3	86.0	23.0	161.0	9.5	62.0	0.2
540	18.2	15.0	3.4	$5.0 \times 10^9$	1.00	5.00	14.0	41.0	14.0	54.0	12.0	62.0	1.5	7.1	0.2
585	17.6	14.0	2.0	$5.5 \times 10^9$	1.00	5.00	6.7	22.0	6.7	37.0	4.9	57.0	0.3	1.8	0.2
630	17.0	13.0	1.5	$4.0 \times 10^9$	1.04	5.37	6.3	17.0	4.8	39.0	2.7	18.0	0.2	0.1	0.2
670	16.4	12.0	0.9	$3.0 \times 10^9$	1.17	5.85	2.0	8.0	0.6	1.7	0.2	6.9	0.1	0.4	0.2

Table C-IX. Shock Layer Attenuation, 40-deg Cone

Time, sec	Altitude, M	Velocity, km/sec	$\frac{I_p}{I_0}$ , Ghz	$\frac{dI_p}{dt}$ , rad/sec	$415 \text{ MHz}$ , m.	Attenuation, dB					Transit, Sec
						$\text{I} \cdot 10^6$ , W	$\text{I} \cdot 250 \text{ MHz}$ , W	$\text{I} \cdot 50 \text{ MHz}$ , W	$\text{I} \cdot 1 \text{ GHz}$ , W	$\text{I} \cdot 10 \text{ GHz}$ , W	
0	300	23.6	$2.05 \times 10^7$	0.44	2.23	7.1	27.0	5.1	19.0	1.1	0.0
100	244	23.0	$3.3 \times 10^6$	0.44	2.20	26.0	73.0	16.0	57.0	2.7	0.2
150	247	24.4	$9.0 \times 10^5$	0.44	2.30	46.0	103.0	35.0	120.0	3.4	2.4
190	246	23.0	$1.3 \times 10^6$	0.50	2.51	38.0	115.0	34.0	117.0	4.4	17.0
230	237	22.6	$1.7 \times 10^6$	0.52	2.42	27.0	118.0	34.0	114.0	4.8	16.0
270	229	21.0	$8.00 \times 10^5$	0.52	2.42	36.0	87.0	26.0	96.0	5.7	1.4
275	229	21.0	$8.00 \times 10^5$	0.52	2.42	36.0	87.0	26.0	96.0	5.7	1.4
320	214	20.0	$6.1 \times 10^6$	0.56	2.02	25.0	78.0	25.0	81.0	6.4	0.5
365	207	19.0	$4.3 \times 10^6$	0.64	1.64	16.0	53.0	14.0	53.0	7.4	0.0
0	300	23.6	$2.05 \times 10^7$	0.44	2.20	7.1	27.0	5.1	19.0	1.1	0.0
30	230	23.6	$4.05 \times 10^6$	0.44	2.20	17.0	52.0	16.0	53.0	6.4	0.0
60	230	23.6	$8.00 \times 10^5$	0.44	2.20	31.0	95.0	28.0	84.0	8.2	5.9
90	230	23.6	$1.4 \times 10^6$	0.44	2.20	44.0	154.0	44.0	157.0	12.0	26.0
120	229	23.6	$2.0 \times 10^6$	0.44	2.20	51.0	147.0	51.0	171.0	14.0	31.0
150	229	23.6	$2.6 \times 10^6$	0.44	2.20	47.0	150.0	61.0	200.0	17.0	39.0
170	226	23.6	$3.4 \times 10^6$	0.44	2.20	47.0	150.0	60.0	180.0	20.0	49.0
205	209	24.0	$5.9 \times 10^5$	0.46	2.30	41.0	128.0	50.0	174.0	23.4	23.4
240	203	23.0	$9.0 \times 10^5$	0.50	2.71	41.0	121.0	43.0	141.0	25.0	25.0
275	200	22.0	$16.00 \times 10^5$	0.52	2.62	36.0	117.0	33.0	104.0	29.0	49.0
305	200	21.0	$4.0 \times 10^6$	0.52	2.62	36.0	92.0	26.0	121.0	32.0	76.0
340	200	20.0	$3.7 \times 10^6$	0.54	2.82	26.0	78.0	23.0	76.0	35.0	7.0
375	200	19.0	$3.1 \times 10^6$	0.61	2.82	17.0	48.0	16.0	59.0	44.0	2.4
410	200	18.0	$3.00 \times 10^6$	0.63	3.14	12.0	37.0	10.0	34.0	41.0	0.0
450	194	17.0	$3.3 \times 10^6$	0.65	3.24	4.4	18.0	4.0	21.0	17.0	0.0
495	186	16.0	$3.3 \times 10^6$	0.69	3.45	1.6	9.0	1.7	9.0	6.4	0.0
540	182	15.0	$0.90 \times 10^6$	0.75	3.77	2.6	6.6	1.3	8.0	4.1	0.0
585	176	14.0	$3.9 \times 10^6$	0.82	4.08	1.3	4.7	0.8	4.5	1.7	0.0
625	170	13.0	$3.9 \times 10^6$	0.90	4.50	0.6	3.0	0.4	2.2	0.8	0.0
670	164	12.0	$4.1 \times 10^6$	0.94	4.70	0.2	0.8	0.1	0.7	0.0	0.0

Table C-X. Boundary Layer Attenuation, 40-deg Cone

Time, sec	Altitude, ft	Velocity, ft/sec	$\frac{V_p}{V}$ , GHz	dis. in. 10 <sup>3</sup>	dis. in. 10 <sup>3</sup>	Attenuation, dB										Trans. Eqn.	Trans.
						f = 150 MHz 1/T	f = 1 GHz 1/T	f = 500 MHz 1/T	f = 1 GHz 1/T	f = 5 GHz 1/T	f = 10 GHz 1/T						
0	300	25.6	-	-	-	-	-	-	-	-	-	-	-	-	-	-	-
100	266	25.0	-	$9.3 \times 10^3$	0.19	0.42	20.0	43.0	26.0	36.0	19.0	11.0	6.8	10.00	2.5	10.0	
150	247	24.0	(2.3)	-	-	-	-	-	-	-	-	-	-	-	-	-	-
190	236	23.0	11.0	$1.65 \times 10^3$	0.16	0.35	24.0	34.0	22.0	31.0	14.0	21.0	1.5	6.3	-	-	-
230	227	22.0	9.4	$2.0 \times 10^3$	0.13	0.30	18.0	31.0	16.0	23.0	12.0	20.0	2.0	7.30	0.4	1.5	-
270	220	21.0	7.0	$2.5 \times 10^3$	0.12	0.27	12.0	18.0	11.0	17.0	6.3	11.0	0.7	2.30	0.1	0.3	-
310	214	20.0	5.3	$3.0 \times 10^3$	0.11	0.25	7.5	12.7	6.0	10.0	3.5	7.0	5.3	0.30	0.0	0.1	-
350	207	19.0	3.7	$3.7 \times 10^3$	0.10	0.22	3.0	7.0	3.0	6.0	1.5	3.0	0.1	0.25	0.3	0.0	-
365	-	-	-	-	-	-	-	-	-	-	-	-	-	-	-	-	-
0	300	25.6	-	-	-	-	-	-	-	-	-	-	-	-	-	-	-
30	289	25.6	-	-	-	-	-	-	-	-	-	-	-	-	-	-	-
60	269	25.6	-	-	-	-	-	-	-	-	-	-	-	-	-	-	-
90	249	25.6	23.00	$1.45 \times 10^3$	0.160	0.35	30.0	54.0	36.0	64.0	32.0	52.0	17.0	16.0	16.0	30.0	2
120	229	25.6	34.00	$3.1 \times 10^3$	0.110	0.24	26.0	47.0	34.0	51.0	35.0	51.0	26.0	46.0	16.0	33.0	2
150	209	25.6	51.00	$6.4 \times 10^3$	0.073	0.16	31.0	42.0	34.0	44.0	34.0	44.0	24.0	44.0	16.0	37.0	2
170	200	25.6	43.00	$6.3 \times 10^3$	0.074	0.17	26.0	39.0	31.0	42.0	30.0	40.0	20.0	40.0	16.0	34.0	2
200	199	24.0	32.00	$6.0 \times 10^3$	0.074	0.17	26.0	34.0	24.0	35.0	25.0	35.0	15.0	29.0	16.0	28.0	2
230	199	23.0	24.00	$5.7 \times 10^3$	0.074	0.18	22.0	32.0	18.0	30.0	18.0	31.0	7.0	22.0	1.3	16.0	2
270	200	22.0	16.00	$5.4 \times 10^3$	0.068	0.18	17.0	23.0	13.0	21.0	13.0	23.0	5.0	11.0	1.6	5.0	2
300	211	16.00	10.50	$5.2 \times 10^3$	0.064	0.19	12.0	18.0	9.0	15.0	9.0	15.0	1.5	4.5	0.2	1.0	2
340	200	20.0	6.70	$4.8 \times 10^3$	0.066	0.19	7.0	12.0	4.5	9.0	6.0	9.0	0.5	1.5	0.2	0.5	2
375	200	19.0	4.30	$4.6 \times 10^3$	0.064	0.20	3.7	8.3	3.0	6.5	1.0	6.5	0.0	0.3	0.0	0.1	2
410	200	18.0	2.60	$4.3 \times 10^3$	0.071	0.20	1.0	4.0	1.0	2.0	0.4	2.0	0.1	0.0	0.0	0.0	2
450	194	17.0	1.30	$5.3 \times 10^3$	0.062	0.18	0.6	1.3	0.5	0.8	0.2	0.5	0.0	0.0	0.0	0.0	2
495	184	16.0	1.95	$5.0 \times 10^3$	0.060	0.18	0.2	0.4	0.1	0.2	0.1	0.2	0.0	0.0	0.0	0.0	2
540	182	15.0	0.64	$6.7 \times 10^3$	0.074	0.17	0.1	0.2	0.0	0.1	0.0	0.1	0.0	0.0	0.0	0.0	2
585	176	14.0	0.33	$7.4 \times 10^3$	0.072	0.16	0.0	0.0	0.0	0.0	0.0	0.0	0.0	0.0	0.0	0.0	2
625	170	13.0	0.16	$8.1 \times 10^3$	0.067	0.15	0.0	0.0	0.0	0.0	0.0	0.0	0.0	0.0	0.0	0.0	2
670	164	12.0	-	-	-	-	-	-	-	-	-	-	-	-	-	-	2

Table C-XI. Shock Layer Attenuation, 30-deg Cone

Time, sec	Altitude, ft	Velocity, ft/sec	$\frac{1}{2} \cdot \frac{1}{\rho}$ , dyn/cm <sup>2</sup>	dF/dt, dyn/sec	dF/dt, dyn	Attenuation, dB						Project. 1 - Eqn.	Project. 2 - Trans.
						100 MHz	1 GHz	10 GHz	100 GHz	1 THz	10 THz		
0	160	21.6	0.59	$1.1 \times 10^7$	0.34	0.10	0.11	0.11	0.11	0.11	0.11	0.0	0.0
160	21.6	23.0	1.10	$1.9 \times 10^7$	0.44	0.19	0.19	0.19	0.19	0.19	0.19	0.0	0.0
150	21.7	24.0	1.20	$5.0 \times 10^7$	0.40	0.17	0.19	0.19	0.19	0.19	0.19	0.0	0.0
140	21.8	23.0	0.60	$7.1 \times 10^7$	0.42	0.18	0.18	0.18	0.18	0.18	0.18	0.0	0.0
130	21.9	22.0	0.65	$1.0 \times 10^8$	0.44	0.20	0.20	0.20	0.20	0.20	0.20	0.0	0.0
120	21.9	21.0	0.55	$1.1 \times 10^8$	0.44	0.20	0.20	0.20	0.20	0.20	0.20	0.0	0.0
110	21.9	20.0	0.50	$1.2 \times 10^8$	0.44	0.19	0.19	0.19	0.19	0.19	0.19	0.0	0.0
100	21.9	19.0	0.45	$1.3 \times 10^8$	0.32	0.18	0.18	0.18	0.18	0.18	0.18	0.0	0.0
90	21.9	20.0	0.50	$2.5 \times 10^7$	0.32	0.18	0.18	0.18	0.18	0.18	0.18	0.0	0.0
80	21.9	21.0	0.50	$9.0 \times 10^7$	0.34	0.18	0.18	0.18	0.18	0.18	0.18	0.0	0.0
70	21.9	21.0	0.50	$2.0 \times 10^8$	0.34	0.18	0.18	0.18	0.18	0.18	0.18	0.0	0.0
60	21.9	21.0	0.50	$7.9 \times 10^8$	0.38	0.18	0.18	0.18	0.18	0.18	0.18	0.0	0.0
50	21.9	21.0	0.50	$1.2 \times 10^9$	0.40	0.18	0.18	0.18	0.18	0.18	0.18	0.0	0.0
40	21.9	21.0	0.50	$1.6 \times 10^9$	0.40	0.18	0.18	0.18	0.18	0.18	0.18	0.0	0.0
30	21.9	21.0	0.50	$1.6 \times 10^9$	0.40	0.18	0.18	0.18	0.18	0.18	0.18	0.0	0.0
20	21.9	21.0	0.50	$1.6 \times 10^9$	0.40	0.18	0.18	0.18	0.18	0.18	0.18	0.0	0.0
10	21.9	21.0	0.50	$1.6 \times 10^9$	0.40	0.18	0.18	0.18	0.18	0.18	0.18	0.0	0.0
0	21.9	21.0	0.50	$1.6 \times 10^9$	0.40	0.18	0.18	0.18	0.18	0.18	0.18	0.0	0.0
410	200	18.0	0.35	$1.7 \times 10^7$	0.54	2.72	0.32	1.4	0.1	0.7	0.0	0.0	0.0
450	194	17.0	0.30	$2.0 \times 10^7$	0.58	2.92	0.24	1.1	0.1	0.6	0.0	0.0	0.0
495	188	16.0	0.15	$2.0 \times 10^7$	0.61	3.03	0.19	0.4	0.0	0.2	0.0	0.0	0.0
540	182	15.0	0.13	$2.1 \times 10^7$	0.63	3.25	0.00	0.2	0.0	0.1	0.0	0.0	0.0
585	176	14.0	0.08	$2.2 \times 10^7$	0.71	3.55	0.00	0.1	0.0	0.0	0.0	0.0	0.0
630	170	13.0	-	-	-	-	-	-	-	-	-	-	-
670	164	12.0	-	-	-	-	-	-	-	-	-	-	-

Table C-XII. Boundary Layer Attenuation, 30-deg Cone

Time, sec	Altitude, h.ft.	Velocity, hft/sec	$\frac{V}{c}$ , Ghz	Velocity rad/sec	dist, in. in.	dist, in. in.	Attenuation, dB						Project. Eqn. Trans.
							1 h - 250 MHz	1 h - 320 MHz	1 h - 1 GHz	1 h - 5 GHz	1 h - 10 GHz	1 h - 20 GHz	
0	360	25.6	-	-	-	-	-	-	-	-	-	-	-
160	264	25.6	-	-	-	-	-	-	-	-	-	-	-
150	267	26.0	$6.4 \times 10^3$	0.22	0.50	0.1	15.60	4.7	16.0	1.4	9.0	0.0	0.0
190	234	23.0	$1.0 \times 10^3$	0.10	0.41	0.7	11.80	2.0	9.0	1.3	3.0	0.0	0.0
230	217	22.0	$1.4 \times 10^3$	0.10	0.34	3.1	6.70	1.6	2.6	0.3	0.0	0.0	0.0
270	200	21.0	$1.8 \times 10^3$	0.14	0.34	1.2	3.20	0.7	1.3	0.3	0.0	0.0	0.0
310	214	20.0	$2.1 \times 10^3$	0.13	0.30	0.3	0.95	0.4	0.9	0.1	0.0	0.0	0.0
350	207	19.0	$2.4 \times 10^3$	0.12	0.27	0.1	0.60	0.1	0.4	0.0	0.0	0.0	0.0
0	360	25.4	-	-	-	-	-	-	-	-	-	-	-
20	260	25.4	-	-	-	-	-	-	-	-	-	-	-
40	260	25.4	-	-	-	-	-	-	-	-	-	-	-
90	244	25.4	$7.7 \times 10^3$	0.190	0.43	21.0	29.0	9.0	16.0	0.3	1.6	0.4	0.2
120	230	25.4	$10.0 \times 10^3$	0.150	0.30	19.0	26.0	16.0	22.0	11.0	2.0	7.0	2.0
150	209	25.4	$13.5 \times 10^3$	0.095	0.19	10.0	25.0	16.0	24.0	14.0	3.9	11.0	1.7
170	200	25.0	$12.5 \times 10^3$	0.080	0.20	16.0	21.0	14.0	21.0	19.0	2.5	6.0	2.0
200	200	24.0	$12.7 \times 10^3$	0.070	0.20	11.0	17.0	7.0	11.0	11.0	1.2	3.5	0.2
240	200	23.0	$13.7 \times 10^3$	0.060	0.21	6.7	13.0	5.7	10.0	1.3	0.4	0.0	0.4
270	200	22.0	$13.0 \times 10^3$	0.050	0.21	3.0	6.7	3.0	6.0	1.7	0.0	0.0	0.1
300	200	21.0	$12.4 \times 10^3$	0.040	0.22	1.6	3.3	1.3	1.4	0.0	0.0	0.0	0.0
335	200	20.0	$11.9 \times 10^3$	0.030	0.23	0.7	1.0	0.9	1.2	0.1	0.0	0.0	0.0
370	200	19.0	$11.5 \times 10^3$	0.020	0.24	0.3	0.6	0.2	0.4	0.0	0.0	0.0	0.0
410	200	-	-	-	-	-	-	-	-	-	-	-	-
450	194	-	-	-	-	-	-	-	-	-	-	-	-
495	186	-	-	-	-	-	-	-	-	-	-	-	-
540	184	-	-	-	-	-	-	-	-	-	-	-	-
585	176	-	-	-	-	-	-	-	-	-	-	-	-
625	170	-	-	-	-	-	-	-	-	-	-	-	-
670	164	-	-	-	-	-	-	-	-	-	-	-	-

Table C-XIII. Boundary Layer Attenuation, 20-deg Cone

Time, sec	Altitude, ft	Velocity, ft/sec	$\frac{f_0}{C}$ , ft/sec	41 ft/s, in.	Attenuation, dB				Project # 77-4001
					100 MPH	140 MPH	180 MPH	220 MPH	
0	100	25.6	-	-	-	-	-	-	-
100	264	25.0	-	-	-	-	-	-	-
150	247	24.0	$0.89 \times 10^{-3}$	0.10	0.48	0.7	1.0	1.3	-
190	234	23.0	$0.74 \times 10^{-3}$	0.15	0.55	0.8	1.1	1.4	-
210	227	22.0	$0.61 \times 10^{-3}$	0.22	0.64	0.9	1.2	1.5	-
215	220	21.0	$0.44 \times 10^{-3}$	0.28	0.64	0.9	1.2	1.5	-
219	214	20.0	$0.31 \times 10^{-3}$	0.18	0.49	0.61	0.8	1.0	-
265	207	19.0	$0.22 \times 10^{-3}$	0.16	0.36	0.4	0.5	0.6	-
300	25.6	-	-	-	-	-	-	-	-
30	260	25.6	-	-	-	-	-	-	-
45	260	25.6	-	-	-	-	-	-	-
90	240	25.6	$2.80 \times 10^{-3}$	0.26	0.59	0.9	1.3	1.7	-
120	230	25.6	$2.90 \times 10^{-3}$	0.17	0.39	0.53	0.68	0.8	-
150	200	25.6	$4.20 \times 10^{-3}$	0.12	0.27	0.39	0.5	0.7	-
170	200	25.0	$3.40 \times 10^{-3}$	0.12	0.27	0.37	0.4	0.5	-
205	200	24.0	$4.50 \times 10^{-3}$	0.12	0.27	0.33	0.4	0.5	-
240	200	23.0	$1.60 \times 10^{-3}$	0.13	0.28	0.38	0.48	0.6	-
275	200	22.0	$1.10 \times 10^{-3}$	0.13	0.29	0.37	0.44	0.5	-
305	200	21.0	$0.67 \times 10^{-3}$	0.14	0.30	0.3	0.3	0.4	-
340	200	20.0	$0.42 \times 10^{-3}$	0.14	0.31	0.2	0.1	0.2	-
375	200	19.0	$0.26 \times 10^{-3}$	0.14	0.32	0.1	0.0	0.0	-
410	200	18.0	$0.15 \times 10^{-3}$	0.14	0.32	0.0	0.0	0.0	-
450	194	17.0	-	-	-	-	-	-	-
495	184	16.0	-	-	-	-	-	-	-
540	182	15.0	-	-	-	-	-	-	-
585	178	14.0	-	-	-	-	-	-	-
625	170	13.0	-	-	-	-	-	-	-
670	164	12.0	-	-	-	-	-	-	-

Table C-XIV. Shock Layer Thickness vs Ionization Distance for Cones and Wedges

Time, sec	Altitude, in.	Velocity, in./sec	10-deg. cone			45-deg. cone			90-deg. cone			10-deg. wedge			45-deg. wedge			90-deg. wedge		
			at 10°	at 45°	at 90°	at 10°	at 45°	at 90°	at 10°	at 45°	at 90°	at 10°	at 45°	at 90°	at 10°	at 45°	at 90°	at 10°	at 45°	at 90°
0	300	25.6	0.33	1.63	210.0	0.44	2.23	>10.0	0.52	2.42	>10.0	0.73	3.44	210.0	0.90	4.50	210.0	1.04	5.22	210.0
100	250	25.6	0.30	1.59	210.0	0.44	2.20	6.0	0.54	2.72	3.00	0.73	3.64	210.0	0.90	4.50	4.0	1.04	5.44	2.9
150	247	24.9	0.40	1.69	210.0	0.44	2.30	2.5	0.56	2.92	1.00	0.75	3.77	8.0	0.94	6.71	2.2	1.17	5.85	0.9
190	230	23.0	0.32	2.10	210.0	0.50	2.51	2.0	0.58	2.92	0.70	0.80	3.90	7.0	0.90	6.92	1.0	1.17	5.95	0.7
230	227	22.0	0.44	2.30	190.0	0.52	2.62	1.5	0.58	2.92	0.80	0.84	4.18	6.0	1.04	5.22	1.3	1.24	6.14	0.5
275	220	21.0	0.44	2.30	-	0.52	2.62	1.5	0.65	2.75	0.70	0.86	4.30	6.0	1.04	5.22	1.3	1.34	6.72	0.4
320	214	20.0	0.44	2.40	-	0.56	2.82	1.5	0.71	2.56	0.70	0.92	4.40	7.0	1.07	5.34	1.3	1.34	6.90	0.3
360	207	19.0	0.32	2.60	-	0.61	3.01	2.0	0.77	2.65	0.75	0.96	4.50	-	1.13	5.65	1.5	1.44	7.31	0.1
400	200	25.6	0.30	1.63	210.0	0.44	2.20	>10.0	0.52	2.42	>10.0	0.73	3.44	210.0	0.90	4.50	210.0	1.04	5.22	210.0
450	200	25.6	0.30	1.63	210.0	0.44	2.20	10.0	0.52	2.62	6.00	0.73	3.64	210.0	0.90	4.50	210.0	1.04	5.22	4.50
500	200	25.6	0.30	1.63	210.0	0.44	2.20	6.0	0.52	2.82	1.50	0.75	3.84	10.0	0.90	4.50	210.0	1.04	5.22	1.50
550	200	25.6	0.30	1.63	210.0	0.44	2.20	1.5	0.52	2.82	0.60	0.73	3.84	6.0	0.90	4.50	210.0	1.04	5.22	0.50
600	200	25.6	0.30	1.63	210.0	0.44	2.20	1.5	0.52	2.82	0.60	0.73	3.84	6.0	0.90	4.50	210.0	1.04	5.22	0.23
650	200	25.6	0.30	1.63	210.0	0.44	2.20	1.5	0.52	2.82	0.60	0.73	3.84	6.0	0.90	4.50	210.0	1.04	5.22	0.10
700	200	25.6	0.30	1.63	210.0	0.44	2.20	>10.0	0.52	2.82	>10.0	0.73	3.84	210.0	0.90	4.50	210.0	1.04	5.22	0.11
750	200	25.6	0.30	1.63	210.0	0.44	2.20	10.0	0.52	2.82	6.00	0.73	3.84	210.0	0.90	4.50	210.0	1.04	5.22	0.25
800	200	25.6	0.30	1.63	210.0	0.44	2.20	6.0	0.52	2.82	1.50	0.73	3.84	10.0	0.90	4.50	210.0	1.04	5.22	0.15
850	200	25.6	0.30	1.63	210.0	0.44	2.20	1.5	0.52	2.82	0.60	0.73	3.84	6.0	0.90	4.50	210.0	1.04	5.22	0.05
900	200	25.6	0.30	1.63	210.0	0.44	2.20	1.5	0.52	2.82	0.60	0.73	3.84	6.0	0.90	4.50	210.0	1.04	5.22	0.02
950	200	25.6	0.30	1.63	210.0	0.44	2.20	>10.0	0.52	2.82	>10.0	0.73	3.84	210.0	0.90	4.50	210.0	1.04	5.22	0.01
1000	200	25.6	0.30	1.63	210.0	0.44	2.20	10.0	0.52	2.82	6.00	0.73	3.84	210.0	0.90	4.50	210.0	1.04	5.22	0.00
1050	200	25.6	0.30	1.63	210.0	0.44	2.20	6.0	0.52	2.82	1.50	0.73	3.84	10.0	0.90	4.50	210.0	1.04	5.22	0.00
1100	200	25.6	0.30	1.63	210.0	0.44	2.20	1.5	0.52	2.82	0.60	0.73	3.84	6.0	0.90	4.50	210.0	1.04	5.22	0.00
1150	200	25.6	0.30	1.63	210.0	0.44	2.20	>10.0	0.52	2.82	>10.0	0.73	3.84	210.0	0.90	4.50	210.0	1.04	5.22	0.00
1200	200	25.6	0.30	1.63	210.0	0.44	2.20	10.0	0.52	2.82	6.00	0.73	3.84	210.0	0.90	4.50	210.0	1.04	5.22	0.00
1250	200	25.6	0.30	1.63	210.0	0.44	2.20	6.0	0.52	2.82	1.50	0.73	3.84	10.0	0.90	4.50	210.0	1.04	5.22	0.00
1300	200	25.6	0.30	1.63	210.0	0.44	2.20	1.5	0.52	2.82	0.60	0.73	3.84	6.0	0.90	4.50	210.0	1.04	5.22	0.00
1350	200	25.6	0.30	1.63	210.0	0.44	2.20	>10.0	0.52	2.82	>10.0	0.73	3.84	210.0	0.90	4.50	210.0	1.04	5.22	0.00
1400	200	25.6	0.30	1.63	210.0	0.44	2.20	10.0	0.52	2.82	6.00	0.73	3.84	210.0	0.90	4.50	210.0	1.04	5.22	0.00
1450	200	25.6	0.30	1.63	210.0	0.44	2.20	6.0	0.52	2.82	1.50	0.73	3.84	10.0	0.90	4.50	210.0	1.04	5.22	0.00
1500	200	25.6	0.30	1.63	210.0	0.44	2.20	1.5	0.52	2.82	0.60	0.73	3.84	6.0	0.90	4.50	210.0	1.04	5.22	0.00
1550	200	25.6	0.30	1.63	210.0	0.44	2.20	>10.0	0.52	2.82	>10.0	0.73	3.84	210.0	0.90	4.50	210.0	1.04	5.22	0.00
1600	200	25.6	0.30	1.63	210.0	0.44	2.20	10.0	0.52	2.82	6.00	0.73	3.84	210.0	0.90	4.50	210.0	1.04	5.22	0.00
1650	200	25.6	0.30	1.63	210.0	0.44	2.20	6.0	0.52	2.82	1.50	0.73	3.84	10.0	0.90	4.50	210.0	1.04	5.22	0.00
1700	200	25.6	0.30	1.63	210.0	0.44	2.20	1.5	0.52	2.82	0.60	0.73	3.84	6.0	0.90	4.50	210.0	1.04	5.22	0.00
1750	200	25.6	0.30	1.63	210.0	0.44	2.20	>10.0	0.52	2.82	>10.0	0.73	3.84	210.0	0.90	4.50	210.0	1.04	5.22	0.00
1800	200	25.6	0.30	1.63	210.0	0.44	2.20	10.0	0.52	2.82	6.00	0.73	3.84	210.0	0.90	4.50	210.0	1.04	5.22	0.00
1850	200	25.6	0.30	1.63	210.0	0.44	2.20	6.0	0.52	2.82	1.50	0.73	3.84	10.0	0.90	4.50	210.0	1.04	5.22	0.00
1900	200	25.6	0.30	1.63	210.0	0.44	2.20	1.5	0.52	2.82	0.60	0.73	3.84	6.0	0.90	4.50	210.0	1.04	5.22	0.00
1950	200	25.6	0.30	1.63	210.0	0.44	2.20	>10.0	0.52	2.82	>10.0	0.73	3.84	210.0	0.90	4.50	210.0	1.04	5.22	0.00
2000	200	25.6	0.30	1.63	210.0	0.44	2.20	10.0	0.52	2.82	6.00	0.73	3.84	210.0	0.90	4.50	210.0	1.04	5.22	0.00
2050	200	25.6	0.30	1.63	210.0	0.44	2.20	6.0	0.52	2.82	1.50	0.73	3.84	10.0	0.90	4.50	210.0	1.04	5.22	0.00
2100	200	25.6	0.30	1.63	210.0	0.44	2.20	1.5	0.52	2.82	0.60	0.73	3.84	6.0	0.90	4.50	210.0	1.04	5.22	0.00
2150	200	25.6	0.30	1.63	210.0	0.44	2.20	>10.0	0.52	2.82	>10.0	0.73	3.84	210.0	0.90	4.50	210.0	1.04	5.22	0.00
2200	200	25.6	0.30	1.63	210.0	0.44	2.20	10.0	0.52	2.82	6.00	0.73	3.84	210.0	0.90	4.50	210.0	1.04	5.22	0.00
2250	200	25.6	0.30	1.63	210.0	0.44	2.20	6.0	0.52	2.82	1.50	0.73	3.84	10.0	0.90	4.50	210.0	1.04	5.22	0.00
2300	200	25.6	0.30	1.63	210.0	0.44	2.20	1.5	0.52	2.82	0.60	0.73	3.84	6.0	0.90	4.50	210.0	1.04	5.22	0.00
2350	200	25.6	0.30	1.63	210.0	0.44	2.20	>10.0	0.52	2.82	>10.0	0.73	3.84	210.0	0.90	4.50	210.0	1.04	5.22	0.00
2400	200	25.6	0.30	1.63	210.0	0.44	2.20	10.0	0.52	2.82	6.00	0.73	3.84	210.0	0.90	4.50	210.0	1.04	5.22	0.00
2450	200	25.6	0.30	1.63	210.0	0.44	2.20	6.0	0.52	2.82	1.50	0.73	3.84	10.0	0.90	4.50	210.0	1.04	5.22	0.00
2500	200	25.6	0.30	1.63	210.0	0.44	2.20	1.5	0.52	2.82	0.60	0.73	3.84	6.0	0.90	4.50	210.0	1.04	5.22	0.00
2550	200	25.6	0.30	1.63	210.0	0.44	2.20	>10.0	0.52	2.82	>10.0	0.73	3.84	210.0	0.90	4.50	210.0	1.04	5.22	

REFERENCE

C-1. S. C. Lin and J. D. Teare, "Rate of Ionization Behind Shock Waves in Air. II. Theoretical Interpretations," Phys. Fluids 6, 355-375 (1963).

## APPENDIX D

### SYSTEM MARGINS

As discussed in Volume I, Section II-D, the free space system margin, which is defined as the amount of plasma attenuation that the reentry vehicle system can tolerate while it effectively transmits information, is a function of frequency. The calculations which lead to the frequency dependence exhibited in Fig. 23 of Volume I are presented here.

The free space system margin  $M$  is given by

$$M = 10^{\log_{10}[(S/N)_0/(S/N)_T]} \quad (D-1)$$

where  $(S/N)_0$  is the signal-to-noise ratio neglecting plasma attenuation and  $(S/N)_T$  is the threshold signal-to-noise ratio. If we take the noise figure of the receiver to be unity, the link equation may be written

$$(S/N)_0 = \left( \frac{\lambda_0}{4\pi R} \right)^2 \frac{P_T G_T G_R}{k T_e \Delta f L} \quad (D-2)$$

where  $\lambda_0$  is the free space wavelength,  $R$  is the range,  $P_T$  is the transmitter power,  $G_T$  is the transmitting antenna gain,  $G_R$  is the receiving antenna gain,  $\Delta f$  is the rf bandwidth,  $L$  represents miscellaneous losses,  $k$  is Boltzmann's constant, and  $T_e$  is an effective noise temperature given by

$$T_e = 290^{\circ}\text{K} + T_A \quad (D-3)$$

where  $T_A$  is the effective antenna temperature.

As discussed in Volume I, parameters were chosen as follows:

$$(S/N)_T = 10$$

$$R = 100 \text{ mi}$$

$$\lambda_0 = 0.03 \text{ to } 300 \text{ m}$$

$$P_T = 1 \text{ W}$$

$$G_T = 1$$

$$f = 300 \text{ kHz}$$

$$L = 10$$

The receiving antenna gain and effective antenna temperature are dependent on frequency, and this dependence is illustrated in Figs. D-1 and D-2. These graphs are intended to be representative rather than to provide ultimate design criteria. The data points of Fig. D-1 were obtained from manufacturer's catalogues and published characteristics. The data of Fig. D-2 were obtained from Refs. D-1, D-2, and D-3. In the frequency range below 10 MHz the noise is largely atmospheric, whereas in the range between 10 MHz and 500 MHz the noise is largely galactic.

The results of the system margin calculation are given in Fig. D-3. As discussed in Volume I, system margins for other transmitter power levels, receiver bandpasses, antenna gains, and ranges can easily be obtained from Fig. D-3 and Eq. (D-2).

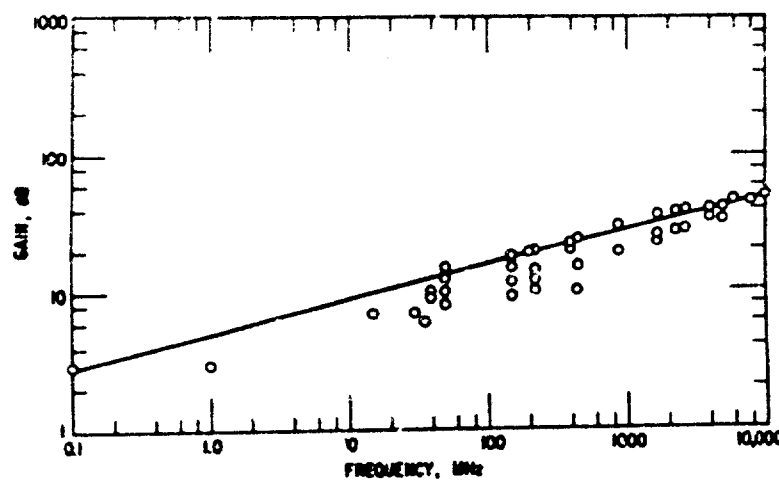


Fig. D-1. Antenna Gain vs Frequency

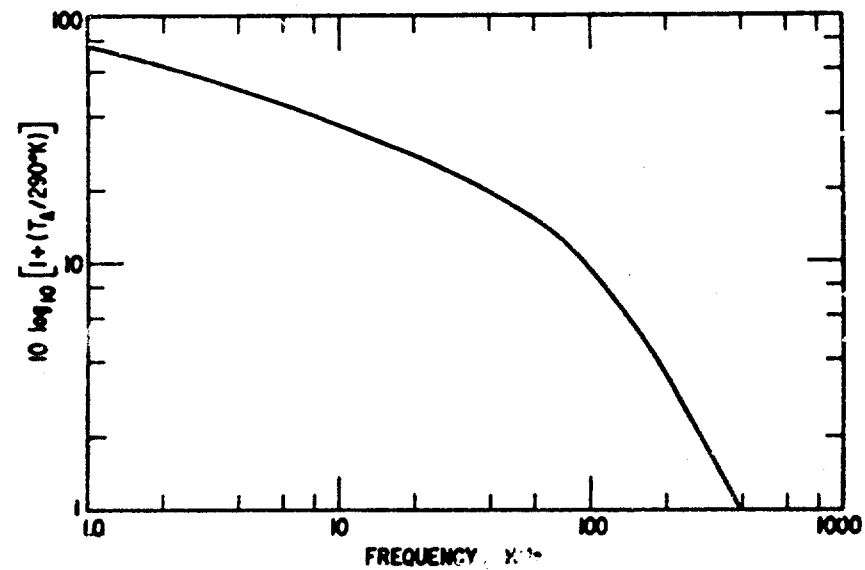


Fig. D-2. Effective Antenna Temperature

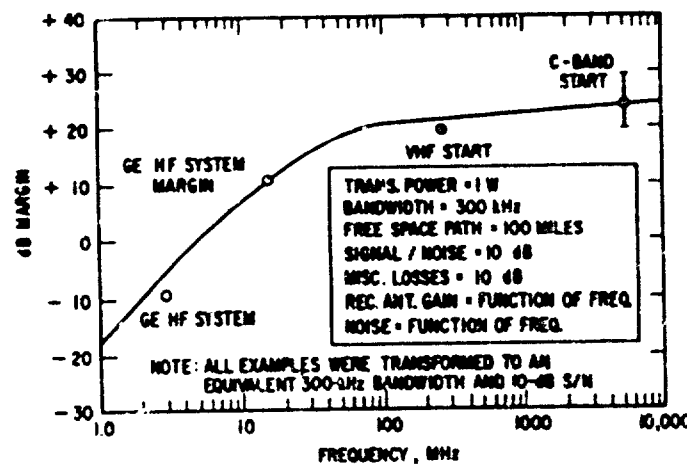


Fig. D-3. Typical Free Space System Margin

## REFERENCES

- D-1. H. L. Stiltz, Aerospace Telemetry Prentice-Hall, Inc., Englewood Cliffs, N.J., (1961). Chap. 7.
- D-2. G. H. Krassner, and J. V. Michaels, Introduction to Space Communication Systems, McGraw-Hill Book Co., Inc., New York (1964). Chap. 4.
- D-3. International Telephone and Telegraph Corporation, Reference Data for Radio Engineers, American Book - Stratford Press, New York (1957). Chap. 25.

## APPENDIX E

### SYSTEM MODIFICATION

Calculations pertinent to the evaluation of the feasibility of increasing the rf power of lifting reentry communications systems are presented in this appendix. The application of the results is presented in Sections III-B, III-D, and III-E of Volume I.

#### 1. POWER AMPLIFIER WEIGHT PENALTY

The weight of a power amplifier over the range of conventional telemetry frequencies may be considered to be directly proportional to both the power output and the operating frequency (Ref. E-1). At 250 MHz, a 6-oz water-cooled tube (EIMAC 4W300B) delivers about 200 W of rf power with an input of about 300 W of dc power. A power supply capable of delivering 300 W for a 10-min period should weigh about 3 lb (this estimate includes batteries and converter). The water required to dissipate 100 W for 10 min is less than 0.1 lb. Allowing 1 lb for the tube and associated components and 3 lb for the power supply, we estimate the total weight for the 200-W amplifier to be 4 lb. Using this estimate for normalization, we derive the relation

$$W = P_o f (1.25 \times 10^4)^{-1} \text{ lb} \quad (\text{E-1})$$

where  $W$  is the weight penalty,  $P_o$  is the output power in W, and  $f$  is the frequency in MHz.

We observe that an EIMAC X-1134 Telemetry Amplifier Package delivers 20 W of CW rf power at 8000 MHz. The package weight is 10 lb, indicating a total weight of 11 lb if we allow 1 lb for a 200-W 28-V source. Our weight-penalty formula gives 13 lb for such a system, and this is taken to indicate that we may use the formula to make sufficiently accurate estimates.

## 2. BREAKDOWN LIMITATIONS FOR PULSED SOURCES

Radio frequency breakdown limitations for CW sources have been discussed in Volume I, Section II-B-4. Here we determine whether breakdown limitations can be reduced by using a source that is pulsed in such a way that average power remains constant while the duty cycle is reduced.

For pulsed rf energy, breakdown occurs when the ionization rate  $v_I$  multiplied by the pulse-length  $\tau$  exceeds a certain constant (Ref. E-2). Since the pulse-length is inversely proportional to the peak power, the power is proportional to the square of the electric field  $E$ , and the ionization rate is a function of the electric field, we conclude that the condition for avoiding breakdown may be written

$$R = \frac{v_I(E)}{E^2} < \text{constant} \quad (\text{E-2})$$

Table E-I, which is based on calculations presented in Ref. E-2, indicates that the quantity  $R$  defined by Eq. (E-2) is an increasing function of peak power and, therefore, a decreasing function of pulse-length. We conclude that breakdown limitations become more severe for a given pulse of electromagnetic energy as the pulse-length is reduced (see Volume I, Section III-B).

Table E-I. Behavior of Breakdown Parameter  $R$

$E$ (relative)	$(E)$ (relative)	$E^2$ (relative)	$R$ (relative)
2	1.5	4	0.4
3	15	9	1.7
4	40	16	2.5
5	150	25	6
10	3000	100	30

## REFERENCES

- E-1. G. E. Mueller, "A Pragmatic Approach to Space Communication," Proc. IRE 48, 557 (1960).
- E-2. A. D. MacDonald, "High Frequency Breakdown of Air at High Altitudes," Proc. IRE 47, 436 (1959).

## APPENDIX F

### COMMUNICATIONS FIN HEAT TRANSFER

In Fig. 25 of Volume I, Section III-C, results of heat transfer calculations are presented to assess the feasibility of the communications fin concept. The relationships used in these calculations are reproduced here. The notation is defined in the referenced literature (Ref. F-1).

#### 1. STAGNATION-LINE HEAT TRANSFER

The heat transfer to the 0.25-in. radius leading edge of the communication fin has been calculated for the entire nonequilibrium trajectory using the following relationship:

$$\dot{q}_{st} = \frac{0.576}{Pr_w^{0.6}} (\rho_e \mu_e)^{0.44} (\rho_w \mu_w)^{0.06} \left( \frac{dU_e}{ds} \right)^{0.5} (h_r - h_w) \left[ 1 + (Le^{0.52} - 1) \frac{h_D}{h_e} \right] \quad (F-1)$$

This expression is a modification, by Kemp, Rose, and Detra (Ref. F-2), of the original relationship given by Fay and Riddell (Ref. F-3). Conditions at the wall were arbitrarily chosen to correspond to  $T_w = 273^{\circ}\text{K}$ .

#### 2. FLAT-PLATE HEAT TRANSFER

The heat transfer to the side of the fin and 1 ft from the leading edge has been calculated using the relationship

$$\dot{q} = 1.383 \frac{k^*}{x} (Re_x^*)^{1/2} (Pr^*)^{1/3} (h_r - h_w) \quad (F-2)$$

where  $k^*$ ,  $Re^*$ , and  $Pr^*$  are evaluated at a temperature  $T^*$  given by

$$T^* = \frac{n^*}{c_p^* \text{ideal}} = \frac{0.28h_e + 0.5h_w + 0.22h_r}{0.24} \quad (F-3)$$

The ideal gas equation of state and the Sutherland viscosity law are assumed. Wall conditions were chosen to correspond to  $T_w = 1300^{\circ}\text{K}$ . Heat transfer rates calculated were compared with the calculations of Miles and Waldman (Ref. F-4) and were found to be in good agreement.

## REFERENCES

- F-1. H. H. Koelle, ed., Handbook of Astronautical Engineering, McGraw-Hill Book Co., Inc., New York (1961).
- F-2. N. H. Kemp, P. H. Rose, and R. W. Detra, Laminar Heat Transfer around Blunt Bodies in Dissociated Air, AVCO Research Lab. Research Rept. 15. (1958)
- F-3. J. A. Fay and F. R. Riddell, "Stagnation Point Heat Transfer in Dissociated Air," AVCO Research Lab. Research Rept. 1 (1957).
- F-4. P. Miles and G. Waldman, Laminar Boundary Layer Skin Friction, Heat Transfer and Displacement Thickness Correlations for Sharp Cones, RAD-TM 62-90, Avco Corp., Research and Advanced Development Div., Wilmington, Mass. (November 1962).

## APPENDIX G

### MAGNETIC WINDOW

Formulas and sample calculations pertinent to magnetic window systems are presented here. The application of these results to the evaluation of magnetic window as a reentry communications system is presented in Volume I, Section III-D.

#### 1. DERIVATION OF FORMULAS

##### a. COIL GEOMETRY

We envision a coil composed of copper or aluminum wire wrapped around a circular antenna aperture. Figure G-1 is a cross-sectional view of the coil showing the average diameter  $d$ , the cross-sectional width  $a$ , the aperture diameter  $b$ , and the distance to the sheath  $y$ .

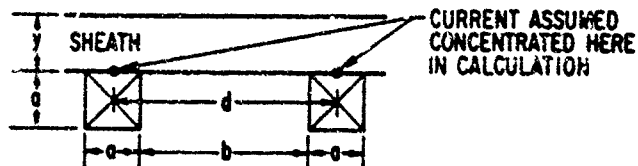


Fig. G-1. Coil Geometry

##### b. CURRENT REQUIREMENT

The total current  $I_T$  in a cross section of the coil is equal to the number of turns in the coil multiplied by the current at the input terminals. The total current requirement is linearly related to the magnetic field strength required in the sheath. For our purposes, this relationship is approximated

by assuming that the equivalent uniform magnetic field of the coil has the same dependence on the displacement  $y$  as the axial field. With this approximation, we obtain

$$\bar{B} \approx \bar{B}_0 \left(1 + \frac{4y^2}{d^2}\right)^{-3/2} \quad (B-1)$$

and to complete the specification of the current requirement we estimate

$$\bar{B}_0 \approx \frac{\mu_0 I}{d} \quad (G-2)$$

In the above expressions,  $\bar{B}$  is the average field in the sheath,  $\bar{B}_0$  is the average field in the plane of the coil, and  $\mu_0$  is the magnetic permeability of free space. (MKS units are used for all quantities except weights, which are given in pounds.)

#### c. SYSTEM WEIGHT AND APERTURE DIAMETER

The total system consists of the coil, the batteries, and the cooling system. If we assign a weight to the coil-supporting structure equal to 10% of the coil weight, and a weight to the cooling system equal to twice the weight of the water required to dissipate ohmic heat losses, we obtain

$$W = \pi d \left[ 1.1 \rho A + \frac{I^2 T_{xt}}{A} \left( \frac{2}{L} + \frac{1}{B} \right) \right] \quad (G-3)$$

where

$W$  = system weight, lb

$\rho$  = specific density of conductor,  $\text{lb/m}^3$

$A = a^2$  = cross-sectional area of coil,  $\text{m}^2$  (see Fig. G-1)

$r$  = resistivity of coil material, ohm-m

$t$  = total time of operation, sec

$L$  = specific heat of vaporization of water, J/lb

$B$  = specific energy capacity of batteries, J/lb

The value of cross-sectional area  $A$  is taken as the value that minimizes the system weight. The minimization procedure yields

$$W = 2.2 \times 10^{-2} I_T d (r \rho t)^{1/2} \text{ lb}$$

$$A = 3.2 \times 10^{-3} I_T (r t / \rho)^{1/2} \text{ m}^2$$

$$b = d - A^{1/2} \text{ m} \quad (G-4)$$

We note that system weight is directly proportional to the magnetic field and the square root of the on-time.

The voltage input  $V_{in}$  and the current input  $I_{in}$  are determined by the number of turns  $N$  in the coil; the number of turns is determined by the size of the coil wire. If the cross-sectional area of the wire is  $\sigma$ , we have

$$N = A / \sigma$$

$$V_{in} = N I_T (r \pi d / A)$$

$$I_{in} = I_T / N \quad (G-5)$$

## 2. SAMPLE CALCULATIONS

Representative requirements for a magnetic window system capable of limiting signal attenuation to 40 dB at a station 1 ft from the apex of a wedge with a 50-deg angle of attack have been presented in Volume I, Section III-C-3-b. The estimated parameters of this system were

$$d = 4 \text{ in.}$$

$$y = 1 \text{ in.}$$

$$\bar{B} = 0.16 \text{ Wb/m}^2 (1600 \text{ G})$$

$$t = 500 \text{ sec}$$

We took the following parameters as representative:

$$L = 10^6 \text{ J/lb}$$

$$B = 1.1 \times 10^5 \text{ J/lb (30 W-h/lb)}$$

$$r = 2.2 \times 10^{-8} \text{ ohm-m (copper)}$$

$$r = 3.9 \times 10^{-8} \text{ ohm-m (aluminum)}$$

$$\rho = 2 \times 10^4 \text{ lb/m}^3 \text{ (copper)}$$

$$\rho = 6 \times 10^3 \text{ lb/m}^3 \text{ (aluminum)}$$

$$\mu_0 = 4\pi \times 10^{-7} \text{ H/m}$$

Using these values in Eq. (G-4), we find that for a copper coil the system weight is about 17 lb, and the aperture diameter is about 2.5 in. For an aluminum coil, the system weight is about 12.5 lb, and the aperture diameter is about 1.5 in.

As indicated in Volume I, Section IV-B, the evaluation of the magnetic field approximations and aperture effects is designated as a task for a future research effort.

## APPENDIX H

### COOLANT INJECTION

The various calculations pertinent to the evaluation of coolant injection as an alleviation technique as described in Volume I, Section III-E, are collected here.

#### 1. PROPERTIES OF COOLANTS

Figure H-1 is adapted from Ref. H-1. The data in the figure are discussed in the argument for the selection of water as an injectant in Volume I, Section III-E-1.

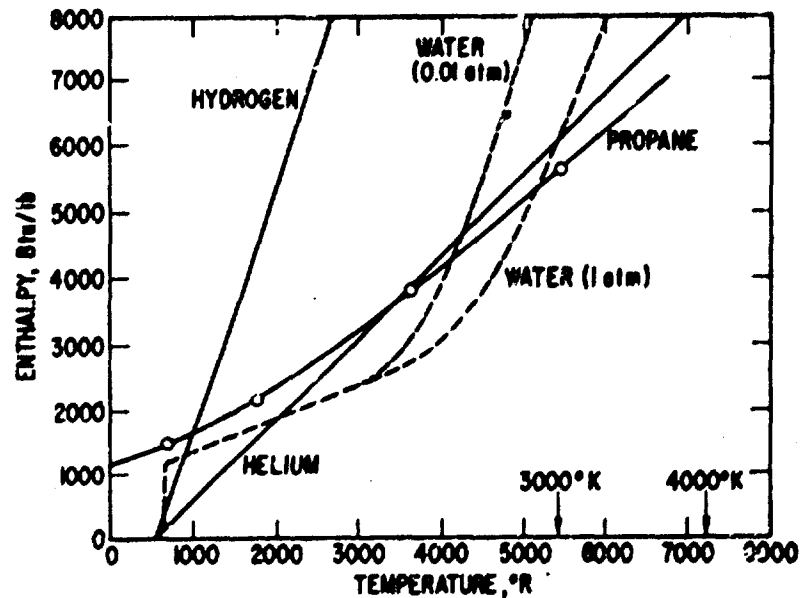


Fig. H-1. Cooling Effectiveness as a Function of Temperature for Various Coolants

2. QUASI ONE-DIMENSIONAL CONSTANT-PRESSURE MIXING PROCESS

As pointed out in Volume I, Section III-E-2-b, we use a technique identical to that of Ref. H-1.

Consider injection into a streamtube as indicated in Fig. H-2.

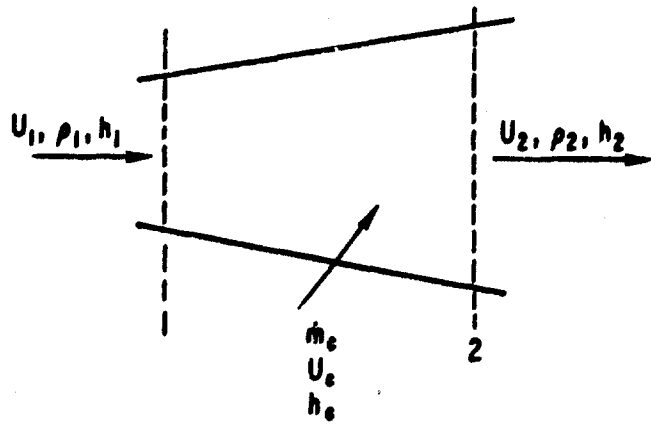


Fig. H-2. Quasi One-Dimensional Mixing Process

The properties are assumed uniform across the cross sections of the streamtube at Stations 1 and 2. The conservation equations are (we assume  $U_c \approx 0$ )

$$\rho_1 U_1^2 A_1 = \rho_2 U_2^2 A_2 \quad (H-1)$$

$$\rho_1 U_1 A_1 + \dot{m}_c = \rho_2 U_2 A_2 \quad (H-2)$$

$$\rho_1 U_1 A_1 \left[ h_1 + \frac{1}{2} (U_1^2) \right] + \dot{m}_c h_c = \rho_2 U_2 A_2 \left[ h_2 + \frac{1}{2} (U_2^2) \right] \quad (H-3)$$

where  $\rho$  is the density;  $U$  is the velocity,  $h$  is the enthalpy,  $\dot{m}_c$  is the injection rate, and  $A$  is the cross-sectional area. We now specifically define

$$C = \frac{\rho_{c_2}}{\rho_2} = \text{mass fraction of coolant at Station 2}$$

$$\rho_{c_2} = \text{density of coolant at Station 2}$$

$$\rho_{a_2} = \text{density of air at Station 2}$$

$$C_Q = \frac{\dot{m}_c}{\rho_1 A_1 U_1} = \text{mass ratio of injectant to incoming flow}$$

Noting that  $C = C_Q / (1 + C_Q)$ , we obtain

$$h_2 = [1 / (1 + C_Q)] [h_1 + C (U_1^2 / 2) + C_Q h_c] \quad (H-4)$$

Thus, for a given state at Station 1 and an injection ratio  $C_Q$ , we may calculate the enthalpy at Station 2, and the pertinent properties of the mixture may be deduced. The electron density is obtained from data for equilibrium air as a function of the temperature and the air density. The collision frequency is obtained (approximately) from the data for equilibrium air (Appendix B, Fig. B-4), where it is assumed that the electron-neutral cross section for helium is seven times greater than that of air on a unit mass basis. Hence, the ordinate in Fig. B-4 is interpreted as  $\nu(\rho_0 / \rho_{\text{eff}})$ , where

$$\frac{\rho_{\text{eff}}}{\rho_0} = \frac{\rho_{a_2}}{\rho_0} + 7 \left( \frac{\rho_{c_2}}{\rho_0} \right) = \frac{1 + 6C}{1 - C} \quad (H-5)$$

and the parameter  $\rho / \rho_0$  is interpreted as  $\rho_{a_2} / \rho_0$ . This is an adequate approximation at the low electron densities of interest, since electron-ion interactions do not contribute significantly to the total electron collision frequency.

The calculation of system weight requirements is described in Volume I, Section III-E-2.

### 3. ELECTRONEGATIVES AS CATALYSTS

The relaxation time of air in the presence of an electronegative gas is given by  $(\sigma_A c_e n_E)^{-1}$ , where  $\sigma_A$  is the attachment cross section,  $c_e$  is the mean thermal speed of the electrons, and  $n_E$  is the number density of the electronegative particles. For  $SF_6$ ,  $\sigma_A$  is of the order of  $10^{-16} \text{ cm}^2$  (see Appendix I). For a typical reentry case (say, a local velocity about 15 kft/sec and a local pressure of about 0.01 atm) the equilibration time should be about 50  $\mu\text{sec}$ . To obtain a relaxation time of 5  $\mu\text{sec}$   $n_E$  should be about  $10^{14}/\text{cc}$ . Since  $SF_6$  is about ten times heavier than water, the water weight is about equal to the weight of air, and the air density is about  $10^{17}/\text{cc}$ , we conclude that the injected mixture should contain about a 1% by weight concentration of  $SF_6$  (see Volume I, Section III-F-2-b).

### 4. ESTIMATE OF DROPLET SIZE

The following empirical expressions for droplet sizes in breakup of liquid jets in air streams are taken from Ref. H-2:

$$\bar{D}/D_o = 3.9(We/Re)^{0.25} \quad (H-6)$$

$$D_{\max}/D_o = 22.3(We/Re)^{0.29} \quad (H-7)$$

where

$\bar{D}$  = volume average droplet diameter

$D_{\max}$  = maximum droplet diameter

$D_o$  = orifice diameter

$We = \sigma/D_o \rho_s V_s^2$

$Re = D_o V_s / \nu$

$\sigma$  = surface tension of liquid

$\rho_s$  = air-stream density

$v_s$  = air stream velocity

$v$  = liquid kinematic velocity

For water

$$\sigma = 65 \text{ dyn/cm}$$

$$v = 4.7 \times 10^{-3} \text{ g/sec-cm (at } 60^\circ\text{C)}$$

For

$$D_0 = 0.01 \text{ in.}$$

$$v_s = 4.5 \times 10^5 \text{ cm/sec}$$

$$\rho_s = 1.29 \times 10^{-5} \text{ g/cc}$$

we obtain

$$\bar{D} = 4.45 \mu$$

$$D_{\max} = 10.8 \mu$$

As discussed in Volume I, Section III-E-2-b, we conclude that a reasonable estimate for the droplet size in the air stream is from 5 to 10 $\mu$ .

## 5. EVAPORATION OF WATER DROPLETS

### a. Free Molecular Flow

For a droplet of water in air

$$qd^2 = - \frac{1}{6} \rho L \frac{d}{dt} (d^3) \quad (H-8)$$

where  $q$  is the energy flux,  $d$  is the diameter of the droplet,  $\rho$  is the specific density of water, and  $L$  is the energy per unit mass required for evaporation of water. We readily obtain

$$t_e = \frac{2d_0 L \rho}{q} (1 - f^{1/3}) \quad (H-9)$$

where  $t_e$  is the evaporation time,  $d_0$  is the initial drop diameter, and  $f$  is the ratio of the unevaporated water weight to the initial water weight. The energy flux  $q$  is given by

$$q = \sum_i n_i c_i E_i \quad (H-10)$$

and

$$E_i = 2kT + \frac{1}{2} \phi_i \quad (H-11)$$

where the summation is over species,  $n_i$  is the particle number density,  $c_i$  is the thermal velocity,  $E_i$  is the energy per particle, and  $\phi_i$  is the energy obtained from recombination processes. Taking 5.1 eV as the recombination energy for oxygen, 9.8 eV as the recombination energy for nitrogen, and the concentrations listed in Table H-I, we obtain the results listed in Table H-II.

Table H-I. Species Concentration in Air

T, °K	[N <sub>2</sub> ]	[N]	[O]
5950	0.34	0.37	0.28
4000	0.65	-	0.35

Table H-II. Evaporation Times, Free Molecular Flow

Evaporation, %	$t_e, \mu\text{sec}$	
	5950°K rate	4000°K rate
70	0.062	0.27
80	0.078	0.34
90	0.100	0.44
100	0.190	0.55

b. Continuum Flow

For the continuum case, the energy flux is given by (see Ref. H-3 and references cited therein)

$$q = \frac{N_{Nu} k_f (h_m - h_w)}{dC_{p,w}} \quad (H-12)$$

where

$$N_{Nu} = \frac{2C_{p,m}L}{C_{p,v,f}(h_m - h_w)} \ln \left( 1 + \frac{C_{p,v,f}}{C_{p,m}} \frac{h_m - h_w}{L} \right) \quad (H-13)$$

and

$N_{Nu}$  = Nusselt number

$k_f$  = thermal conductivity of air at  $T_f = \frac{1}{2} (T_{drop} + T_{mixture})$

$h_m$  = enthalpy of mixture

$h_w$  = enthalpy of water

$C_{p,m}$  = frozen specific heat of mixture

$C_{p,v,f}$  = specific heat of vapor at  $T_f$

Assuming

$$C_{p,m} \approx C_{p,v,f}$$

$$L \approx 1000 \text{ Btu/lb}$$

$$h_m - h_w \approx 5600 \text{ Btu/lb}$$

$$k_f \approx 2.2 \times 10^{-5} \text{ Btu/(ft)(sec)}^{\circ}\text{K}$$

$$C_{p,w} \approx 0.24 \text{ Btu/lb}$$

$$\rho \approx 62.4 \text{ lb/ft}^3$$

we readily obtain

$$t_e = 4.9 \times 10^{-5} (1 - f^{2/3}) \quad (H-14)$$

This approximate formula leads to times  $t_e$  of 0.032, 0.038, and 0.049 msec for 80, 90, and 100% evaporation. The application of these results and the results in Appendix H-5-a are discussed in Volume I, Section III-E-2-b.

## 6. DROPLET DYNAMICS

The equation of motion of a droplet parallel to the air stream is taken as

$$-m \frac{d}{dt} (U_{air} - U_{drop}) = \frac{1}{2} C_D \rho_{air} \frac{\pi d^2}{4} (U_{air} - U_{drop})^2 \quad (H-15)$$

where the notation is standard. If the water jet is perpendicular to the flow,  $x$  is the distance along a streamline,  $y$  is the distance perpendicular to the streamline, and  $U_i$  is the initial velocity of the droplets, then

$$\frac{dx}{dt} = U_{air} \left( 1 - \frac{1}{1 + \frac{3}{4} C_D \frac{\rho_{air}}{\rho_{drop}} \frac{U_{air} t}{d}} \right) \quad (H-16)$$

$$\frac{dy}{dt} = U_i \quad (H-17)$$

For  $U_{air} = 15$  kft/sec,  $C_D = 2$ ,  $\rho_{air}/\rho_{drop} = 4 \times 10^{-6}$ ,  $d = 10\mu$ , and a lateral velocity of 150 ft/sec, the following results are obtained

$t, \mu\text{sec}$	$x, \text{cm}$	$y, \text{cm}$
20	0.55	0.1
100	9.7	0.5
200	31.2	1.0

These values are the basis for the conclusion that the lateral spreading of the insectant is not severe (Volume I, Section III-E-2-b).

## REFERENCES

- H-1. R. H. Adams and J. J. Rossi, Research of Aerodynamic Methods of Producing Antenna Windows in a Plasma Sheath, Sci. Rept. No. 1, Mithras Inc. (October 1964).
- H-2. R. D. Ingebo and H. H. Foster, Drop-Size Distribution for Cross-current Breakup of Liquid Jets in Air Streams, TN 4087, NACA (October 1957).
- H-3. I. E. Beckwith and J. K. Huffman, Injection and Distribution of Liquids in the Flow Fields of Blunt Shapes at Hypersonic Speeds, TM X-989, NASA (August 1964).

## APPENDIX I

### ELECTROPHILIC SEEDING

Communication difficulties created by the plasmas that surround spacecraft during atmospheric reentry have stimulated considerable research on the effect of electronegative gas injection on the ionization levels in hot gases. The experiments of Carswell and Cloutier (Ref. I-1) indicate that concentrations of  $SF_6$  on the order of the initial electron concentration are very effective in quenching argon plasmas produced by an rf discharge. Conversely, the experiments of Fuhs (Ref. I-2) and Hoffman and Westbrook (Ref. I-3) indicate that  $SF_6$  is much less effective in argon arc jets and seeded nitrogen-oxygen flame plasmas. Theoretical results in this area have been either specialized (Refs. I-2 and I-4) or inconclusive (Ref. I-3). It will be shown here that equilibrium ionization levels of high-temperature air are not significantly affected by the presence of electronegative species but that nonequilibrium levels can be rapidly driven to equilibrium levels by the electron-attachment and charge-transfer mechanism. These conclusions are consistent with the experimental observations, and they provide the basis for evaluating the usefulness of these mechanisms in Sections III-E, III-F, and III-G of Volume I.

#### 1. EQUILIBRIUM

The equilibrium concentrations of the various species in seeded air for a given temperature and pressure are obtained by simultaneously solving the chemical equilibrium equations associated with the pertinent reactions and the appropriate conservation equations. At the temperatures and pressures of interest, the dominant species in air are  $N_2$ , N,  $O_2$ , O, NO,  $NO^+$ , and  $e^-$ . If X represents the electronegative component, the mixture will also contain  $X, X^+$ , and whatever compounds can be formed by X with N and O. The equilibrium electron density will be a function of temperature, pressure, and initial seed-gas concentration. The exact solution of this problem requires

detailed knowledge of chemistry and use of an electronic computer; the problem is considerably simplified, however, if only the reduction in electron density as a function of seed-gas concentration is required. If the optimistic assumption is made that the electronegative species interact only with electrons, and the reasonable assumption is made that the variations in the concentrations of N and O due to the injection of the electronegative gas are negligible, we obtain

$$\frac{n_e [NO^+]}{[N][O]} = K_I$$

$$\frac{n_e (N_E - N_E^-)}{N_E^-} = K_A$$

$$K_I = \frac{(n_e^0)^2}{[N][O]} \quad (I-1)$$

$$K_A = \left( \frac{2\pi m_e kT}{h^2} \right)^{3/2} \exp(-E_A/kT)$$

$$n_e + N_E^- = [NO^+]$$

where  $n_e^0$  is the initial electron concentration,  $n_e$  is the equilibrium electron concentration,  $N_E$  is the initial electronegative species concentration,  $N_E^-$  is the equilibrium negative ion concentration,  $K_I$  is the chemical equilibrium constant for the ionization reaction,  $K_A$  is the chemical equilibrium constant for the electron attachment reaction,  $E_A$  is the electron affinity of the electronegative species, and the other symbols are standard. These equations lead to

$$\left( \frac{n_e}{n_e^0} \right)^2 = \frac{n_e + K_A}{N_E + n_e + K_A} \approx \frac{K_A}{N_E + K_A} \quad (I-2)$$

This expression differs from the analogous equation of Ref. I-3 because here account has been taken of Le Chatelier's principle — as the electronegative component removes electrons, the reaction  $N + O \rightarrow NO^+ + e^-$  will produce more electrons. Known electron affinities do not exceed 4 V, therefore the limit of the attachment mechanism effectiveness can easily be calculated. Such calculations for 10% concentrations of 4-V electronegative species in air have been performed for temperatures and pressures characteristic of the reentry environment, and the results are presented in Fig. I-1. The curve labelled  $\rho/\rho_0 = 10^{-2}$  compares favorably with exact calculations (Ref. I-4) for 5% concentrations of  $F_2$ , thus indicating the validity of the assumptions described. The electronegative concentrations required for a reentry system were calculated from Eqs. (I-1) and (I-2), and the results are presented in Volume I, Section III-F-2.

## 2. NONEQUILIBRIUM

When the electron density is higher than the equilibrium level, the approach to equilibrium in the presence of an electronegative component is given by

$$\frac{dn_e}{dt} = - \alpha_R n_e^2 - \alpha_A N_E n_e \quad (I-3)$$

where  $\alpha_R$  is the electron-ion recombination rate constant, and  $\alpha_A$  is the electron attachment rate constant. As pointed out by Carswell and Cloutier, we may assume that the rate at which the electronegative component transfers electrons to positive ions is much faster than the attachment rate, thus  $N_E$  may be regarded as a constant. If we make the transformation  $t \rightarrow \alpha_R n_e^0 \tau$  so that, in the absence of the electronegative component, the electron density decays to one-half its initial value when  $\tau = 1$ , we obtain the solutions given in Fig. I-2, where the seeding parameter  $r$  represents the ratio  $\alpha_A N_E / \alpha_R n_e^0$ . The experimental curves presented by Carswell and Cloutier are in agreement with the theoretical curves for a seeded argon plasma when the reasonable

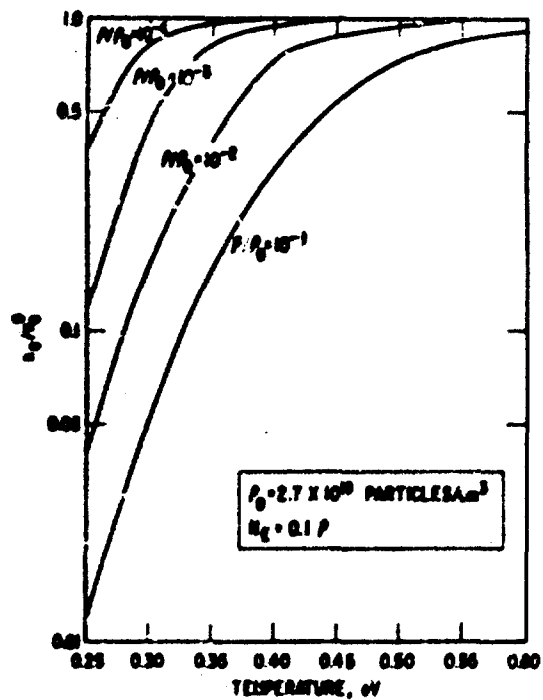
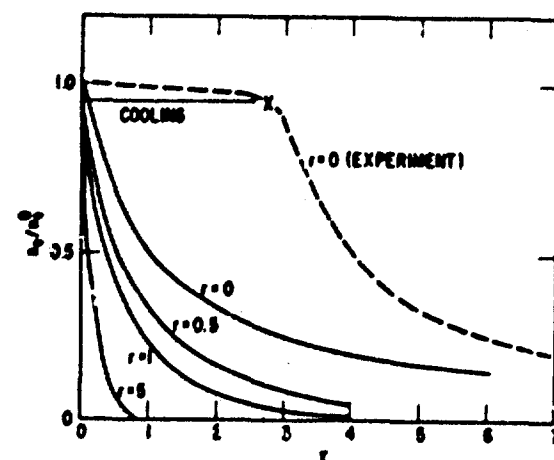


Fig. I-1. Reduction of Equilibrium Electron Concentrations in Seeded Air

Fig. I-2. Reduction of Non-equilibrium Electron Concentrations in Seeded Ionized Gases



assignments  $\alpha_R$ ,  $\alpha_A \sim 10^{-9}$  are made (Refs. I-5 and 6). (The value for  $\alpha_A$  is based on an electron attachment cross section of  $10^{-16} \text{ cm}^2$ .) The dashed line in the figure represents the measured curve for the unseeded plasma — the discrepancy is probably due to the fact that the electrons must be cooled before they can recombine with positive ions (the reported initial temperature was  $7 \times 10^4 \text{ K}$ ).

It may be concluded from these considerations that electrophilic seeding is not effective in reducing equilibrium electron density levels in nonexpanding flows but that it can be effective in catalyzing the electron-ion recombination process in expanding flows or in flows which have been cooled by injection of foreign material. The specific application of these conclusions to the reentry communications problem have been discussed in Volume I, Section III-E, III-F, and III-G.

## REFERENCES

- I-1. A. I. Carswell and G. G. Cloutier, "Supersonic Plasma Streams Seeded with Electronegative Gases," Phys. Fluids 7, 602 (1964).
- I-2. A. E. Fuhs, Thermal Ionization and Electronegative Species, TDR-165(3153)TN-2, Aerospace Corp. (September 1962).
- I-3. J. Hoffman and E. A. Westbrook, "Flame Plasma Seeded with Sulfur Hexafluoride," Phys. Fluids 8, 1410 (1965).
- I-4. A. R. Hochstim, "Electron Concentration in Closed Form For High Temperature Air and Air Additives," Planetary and Space Sciences 6, 79 (1961).
- I-5. I. S. Buchel 'nikova, "Cross Sections for the Capture of Slow Electrons by O<sub>2</sub> and H<sub>2</sub>O Molecules and Molecules of Halogen Compounds," JETP (USSR) 35, 783 (1959).
- I-6. L. B. Loeb, "The Recombination of Ions," Handbuch der Physik, Band XXI, Springer-Verlay, Berlin (1956).

## APPENDIX J

### QUASI-OPTICAL AND OPTICAL SYSTEMS

The power requirements for the systems described in Volume I, Section III-I are derived here.

#### 1. MILLIMETER SYSTEM

The power  $P_R$  required at the input of a state-of-the-art 95-GHz receiver is given by

$$P_R = (S/N)(NF)kT\Delta f \quad (J-1)$$

where

$S/N = 10$  (signal-to-noise power ratio)

$NF = 40$  (receiver noise figure)

$kT = 4 \times 10^{-21} \text{ W/Hz}$  (noise power per cycle)

$\Delta f = 300 \text{ kHz}$  (receiver bandpass)

We readily obtain  $P_R = 4.8 \times 10^{-13} \text{ W}$ . The required output power  $P_T$  for an omnidirectional system is given by

$$P_T = 4\pi (R^2/A_R) P_R \quad (J-2)$$

where  $R$  is the range, and  $A_R$  is the effective area of the receiver antenna.

For a range of 100 miles and an area of  $200 \text{ ft}^2$  we obtain  $P_T = 9 \text{ mW}$ .

Allowing for miscellaneous losses of 10 dB; we estimate a requirement of 90 mW for an omnidirectional clear-weather system. This estimate is discussed in Volume I, Section III-I-1.

## 2. INJECTION LASER SYSTEM

The signal-to-noise ratio at the output of a photomultiplier is given by

$$S/N = \frac{I_S^2}{2e\Delta f(I_S + I_B + I_D)} \quad (J-3)$$

where  $I_S$  is the current due to the signal,  $I_B$  is the current due to the background radiation, and  $I_D$  is the dark current of the tube. In this case, the dark current is negligible, and the required received power is given by

$$P_R = (h\nu/q)(S/N) \Delta f \{ 1 + [ 1 + (2qP_B/h\nu\Delta f)(S/N)^{-1} ]^{1/2} \} \quad (J-4)$$

where  $P_B$  represents the background radiation power,  $h\nu$  is the photon energy,  $q$  is the quantum efficiency of the photomultiplier, and  $\Delta f$  is the bandpass of the video system.

The noise power is given by

$$P_B = I_D \Omega_R A_R B + I_V (A_V/R^2) A_R B \quad (J-5)$$

where

$I_D$  = spectral density of daylight noise  $\approx 10^{-3} \text{ W sr}^{-1} \text{ m}^{-2} \text{ \AA}^{-1}$

$I_V$  = spectral density of vehicle radiation  $\approx 10 \text{ W sr}^{-1} \text{ m}^{-2} \text{ \AA}^{-1}$

$A_R$  = receiving aperture  $\approx 1 \text{ m}^2$

$B$  = optical filter bandpass  $\approx 10 \text{ \AA}$

$\Omega_R$  = receiving field of view  $\approx 10^{-6} \text{ sr}$

using the indicated estimates, we obtain

$$P_D \approx 10^{-8} \text{ W (daylight noise)}$$

$$P_V \approx 2 \times 10^{-8} \text{ W (vehicle noise)}$$

$$P_B \approx 3 \times 10^{-8} \text{ W}$$

Taking  $q \approx 3 \times 10^{-3}$ ,  $h\nu = 2.2 \times 10^{-19} \text{ J}$ , and  $\Delta f = 10^8 \text{ Hz}$  (corresponding to a pulse length of 10 nsec), we obtain  $P_R \approx 3 \times 10^{-8} \text{ W}$ . If atmospheric losses are estimated as 6 dB, a requirement of 50 kW pulses for an omnidirectional transmitting system with a range of 100 miles is indicated. If the transmitted power can be concentrated in a beam with a width of about 10 deg, the peak power requirement is reduced by a factor of about 500, indicating a requirement for 100-W pulses. As discussed in Volume I, Section III-I-2, this estimate is a reasonable requirement for future systems.

## UNCLASSIFIED

Security Classification

## DOCUMENT CONTROL DATA - R&amp;D

(Security classification of title, body of abstract and indexing annotation must be entered when the overall report is classified.)

1. ORIGINATING ACTIVITY (Corporate author) Aerospace Corporation El Segundo, California		2a. REPORT SECURITY CLASSIFICATION Unclassified
		2b. GROUP
3. REPORT TITLE LIFTING REENTRY COMMUNICATIONS: VOLUME II, SYSTEMS CALCULATIONS		
4. DESCRIPTIVE NOTES (Type of report and inclusive dates)		
5. AUTHOR(S) (Last name, first name, initial) Dix, Donald M., Golden, Kurt E., Taylor, Edward C., Koplin, Marc A., and Caron, Paul R.		
6. REPORT DATE September 1966	7a. TOTAL NO OF PAGES 73	7b. NO OF REPS 27
8a. CONTRACT OR GRANT NO AF 04(695)-669	8b. ORIGINATOR'S REPORT NUMBER(S) TR-669(6220-10)-3, Vol II	
9. PROJECT NO c d	9b. OTHER REPORT NO(S) (Any other numbers that may be assigned this report) SSD-TR-66-73, Vol II	
10. AVAILABILITY/LIMITATION NOTICES This document is subject to special export controls and each transmittal to foreign governments or foreign nationals may be made only with prior approval of SSD(SSTRT).		
11. SUPPLEMENTARY NOTES	12. SPONSORING MILITARY ACTIVITY Space Systems Division Air Force Systems Command Los Angeles, California	
13. ABSTRACT  Calculations supporting the lifting reentry communications systems study are described in this volume. The application and interpretation of these calculations is presented in Volume I of this report. These calculations include the study of lifting reentry trajectories, aerodynamic calculations, signal attenuation, system margins, system modifications, communications in heat transfer, magnetic window, cowlant injection, electrophilic seeding, and quasi-optical and optical systems.		

DD FORM 1473  
FACSIMILEUNCLASSIFIED  
Security Classification

**UNCLASSIFIED**

Security Classification

14.

KEY WORDS

Communications Systems  
Reentry Communications  
Lifting Reentry  
Antenna Window  
Aerodynamics  
RF Attenuation  
RF Breakdown  
Aerodynamic Shaping  
Fluid Injection  
Magnetic Window  
Electrophilic Seeding  
Millimeter Waves  
Optical Communications Systems  
High-Frequency Communications  
Communications Blackout

Abstract (Continued)

**UNCLASSIFIED**

Security Classification